Contrib Mineral Petrol (2015) 170:24
DOI 10.1007/s00410-015-1178-8

ORIGINAL PAPER

$^{40}Ar/^{39}Ar$ geochronology, geochemistry and petrology of volcanic rocks from the Simav Graben, western Turkey

Barış Semiz[1] · E. Yalçın Ersoy[2] · Yahya Özpınar[1] · Cahit Helvacı[2] · Martin R. Palmer[3] · Mehmet Z. Billor[4]

Received: 22 March 2015 / Accepted: 28 July 2015 / Published online: 11 August 2015

Abstract Major and trace element compositions with Sr–Nd isotopic ratios, as well as Ar–Ar radiometric ages of the Miocene volcanic rocks from the Neogene units around Simav region (western Anatolia), are used to discuss the genetic relationship between (1) high-voluminous Lower–Middle Miocene high-potassic, calc-alkaline (HKCA) and (2) Middle Miocene small-voluminous high-MgO shoshonitic–ultrapotassic (SHO–UK) magmatic units in the region. All the HKCA rocks, including basaltic to rhyolitic (and granitic) samples, share similar trace element characteristics (enrichments of LILE and LREE and depletions in HFSE as a common feature of orogenic magmatic rocks), with subtle differences in their $^{87}Sr/^{86}Sr_{(i)}$ ratios (basalts and rhyolites ~0.708, dacites ~0.710). Most of the samples of the high-MgO SHO–UK group are classified as shoshonite and latite, with some lamproites, sharing similar geochemical features with the other ultrapotassic rocks of the Mediterranean. All the rock groups have similar and high abundances of incompatible trace elements, and radiogenic Sr. Geochemical modeling of the trace element and isotopic ratios of the samples reveals that both the SHO–UK and HKCA groups were derived from a common mantle source which had been highly metasomatized and enriched by continental materials during partial subduction of the crustal metamorphic slices in a continental collision setting. The geochemical variations of these rocks were mainly controlled by source characteristics (such as heterogeneity) and variable degrees of partial melting and subsequent effects of fractional crystallization, with low degrees of crustal contamination. The HKCA series were derived by higher degrees of partial melting of the lithospheric mantle source than the SHO–UK rocks. The HKCA rocks then underwent two-stage fractional crystallization (clinopyroxene-dominated followed by feldspar-dominated fractionating mineral assemblages) to form the high-K calc-alkaline basalt to rhyolite series, whereas the SHO–UK rocks experienced comparatively little fractional crystallization. A tectonic scenario involving the rapidly extending and thinning of orogenic crust is compatible with the time-dependent compositional variation of the magmatic rocks.

Keywords Geochemistry · Geochronology · Calc-alkaline · Lamproite · Ultrapotassic · Western Anatolia

Communicated by Gordon Moore.

Electronic supplementary material The online version of this article (doi:10.1007/s00410-015-1178-8) contains supplementary material, which is available to authorized users.

✉ Barış Semiz
bsemiz@pau.edu.tr

[1] Department of Geological Engineering, Pamukkale University, 20070 Denizli, Turkey

[2] Department of Geological Engineering, Dokuz Eylül University, 35160 Izmir, Turkey

[3] School of Ocean and Earth Science, NOC, University of Southampton, European Way, Southampton SO14 3ZH, UK

[4] Department of Geology and Geography, Auburn University, Auburn, AL, USA

Introduction

A key feature of the Alpine–Himalayan orogenic system is the presence of post-collisional potassic magmatism, characterized by high-K calc-alkaline rocks (HKCA) and shoshonitic–ultrapotassic (SHO–UK) rocks (e.g., Guo et al.

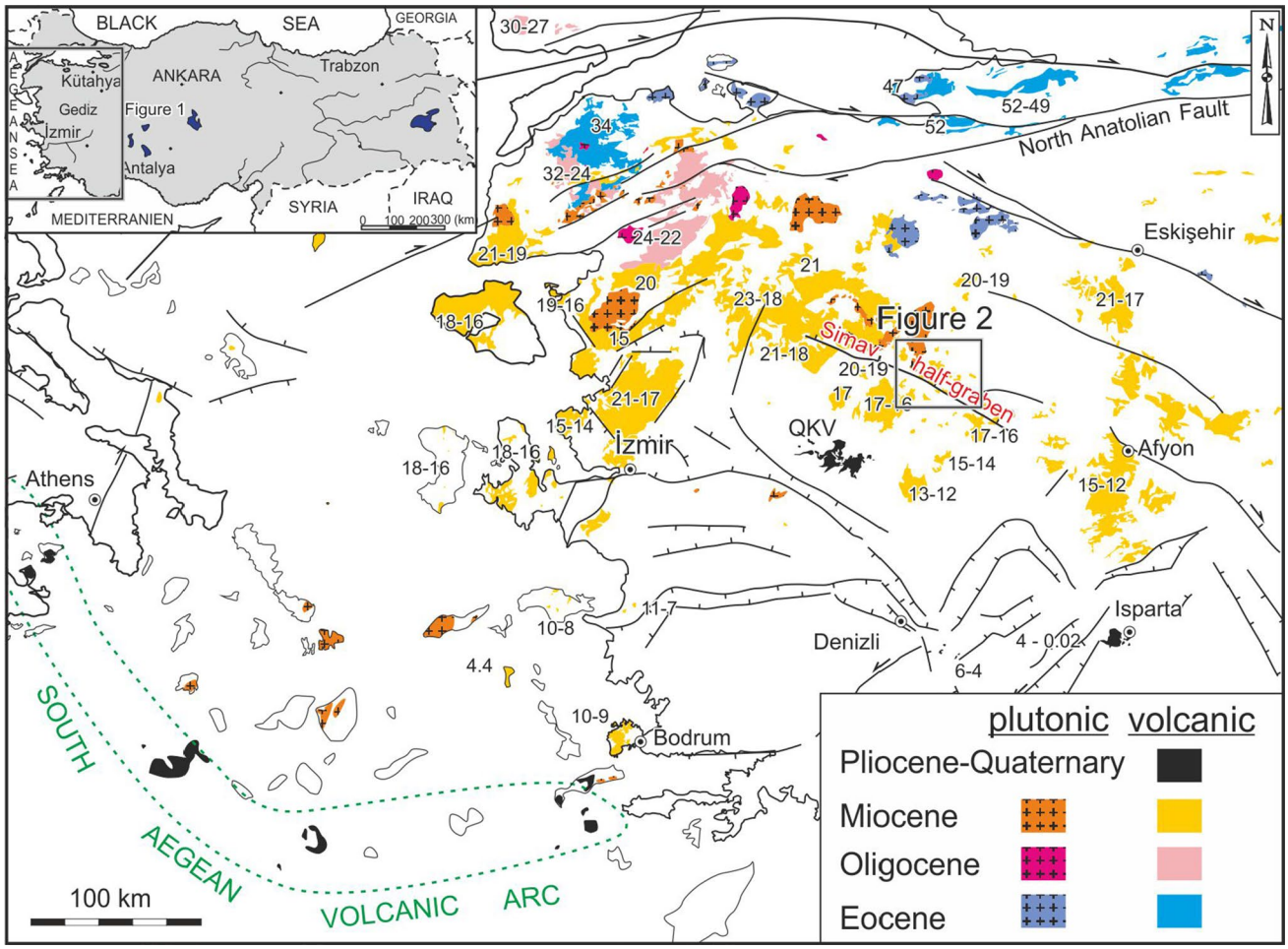

Fig. 1 Geological map of the central Aegean region showing the distribution and ages of the recent magmatism [modified from Ersoy and Palmer (2013)]

2005; Conticelli et al. 2009; Avanzinelli et al. 2009; Lustrino et al. 2011; Ersoy and Palmer 2013). Production of these rocks in post-collisional extensional areas is generally followed by Na-alkaline, OIB-like intra-plate basaltic volcanic activity (Lustrino and Wilson 2007). These magmatic associations are exemplified in western Anatolia, the eastern part of the Aegean extensional system (Ersoy and Palmer 2013), where the region is characterized by widespread Cenozoic magmatic activity which developed after final welding of several tectono-stratigraphic units belonging to the Sakarya Continent to the north, and the Anatolide–Tauride block to the south (Şengör and Yılmaz 1981) (Fig. 1). Cenozoic post-collisional magmatic activity continued, with emplacement of Eocene plutonic and volcanic rocks in the northernmost part of western Anatolia (Altunkaynak and Genç 2008; Kürkçüoğlu et al. 2008; Altunkaynak et al. 2012; Gülmez et al. 2012) and Upper Oligocene–Lower Miocene granitoids and volcanic rocks in the northwestern Anatolia. Magmatic activity continued into the Upper Miocene in the south of the region, with magmatic rocks being emplaced in a belt from the north Aegean islands in the west to the Eskişehir–Afyon region in the east (Fytikas et al. 1984; Pe-Piper and Piper 1989; Richardson-Bunbury 1996; Seyitoğlu et al. 1997; Aldanmaz et al. 2000; Francalanci et al. 2000; Alıcı et al. 2002; Innocenti et al. 2005). In the central parts of western Anatolia, syn-extensional Lower–Middle Miocene granitoids and coeval volcanic rocks are intercalated with lacustrine sediments deposited in extensional basins that were developed at this time (Floyd et al. 1998; Aldanmaz et al. 2000; Innocenti et al. 2005; Karacık et al. 2007; Ersoy and Helvacı 2007; Ersoy et al. 2008, 2010b, 2011; Helvacı et al. 2009; Karaoğlu et al. 2010). These Miocene extensional basins include the NE–SW-trending Demirci, Selendi, Uşak-Güre and Emet supradetachment basins, which were developed on the northern flank of the Menderes Core Complex (MCC) (Ersoy et al. 2008, 2010b, 2012b; Karaoğlu et al. 2010). Post-Miocene extensional tectonics has also led to the formation of ~E–W-trending grabens which cut and displaced the NE–SW-trending Miocene basins (e.g., the Simav half-graben, and the Gediz and

Büyük Menderes grabens (Seyitoğlu et al. 1997; Çiftçi and Bozkurt 2009). The latest phase of collision magmatism in the area lies to the southwest of western Anatolia, where the Pliocene–Quaternary South Aegean Volcanic Arc (SAVA) developed in response to subduction of the African oceanic lithosphere beneath the Aegean plate.

Recent studies of Miocene magmatic activity in the central parts of western Anatolia indicate that three distinct rock groups were produced: (1) Lower–Middle Miocene felsic magmatism associated with the HKCA magmatic series, including granitic plutons and mainly andesitic–rhyolitic volcanics (HKCA), (2) small-volume mafic lava flows with high-MgO shoshonitic–ultrapotassic features and mainly Middle Miocene ages (SHO–UK) and (3) Na-alkaline basalts with OIB-type geochemical features emplaced in the southern part of western Anatolia (Quaternary Kula volcanics, QKV). The petrogenesis of the first two groups has been subject to debate (see Ersoy and Palmer (2013) for a summary), but we hypothesize that the petrogenetic origins of the magmatic groups may be summarized as follows: (1) a hybrid source including metasomatized lithospheric mantle and (lower) crustal reservoirs for the HKCA rocks (e.g., Yılmaz et al. 2001; Ersoy et al. 2012a); (2) a metasomatized lithospheric mantle for the high-MgO SHO–UK rocks (e.g., Yılmaz et al. 2001; Aldanmaz et al. 2000; Ersoy et al. 2010b; Prelević et al. 2012); and (3) an asthenospheric mantle source for the Na-alkaline basaltic rocks (Güleç 1991; Alıcı et al. 2002).

This study aims to explore and test the validity of these models for the petrogenetic evolution of the Miocene HKCA and SHO–UK magmatic activity in the region, using geochronological, petrographic and geochemical data from: (1) the Lower–Middle Miocene HKCA and (2) the Middle Miocene high-MgO SHO–UK magmatic series exposed around the Simav half-graben (Fig. 1). We present new stratigraphic and Ar–Ar age data for the volcanic units, so as to determine their relationship with the NE–SW-trending basins. Whole-rock major and trace element abundances, Sr–Nd isotopic data and mineral chemistry of the volcanic units are also presented and discussed in order to define the petrological evolution of Miocene volcanism in the area, with particular reference to the origin and petrogenetic evolution of the HKCA series, and their genetic relation with the SHO–UK, which is still not well understood.

Analytical techniques

Fresh samples of volcanic rocks were collected from outcrops in the Simav graben. Polished thin sections of samples were studied optically prior to microprobe analyses. Characteristic mineral compositions in rocks from the various units were analyzed on polished sections using the JEOL 8600 electron microprobe at the University of Georgia, USA, following methods described in Roden et al. (2006). During electron microprobe studies, natural and synthetic mineral standards were analyzed as primary standards to monitor accuracy and precision. Running conditions were: 15 kV accelerating voltage, 15 nA beam current and an analytical spot size of ~1 μm. The X-ray intensities were corrected by using PRZ matrix correction software following Armstrong (1988). The mineral chemistry data are listed in Appendix B of Electronic Supplementary Material.

Whole-rock geochemical analyses of 49 representative fresh samples collected from the study area were performed at the ACME Analytical Laboratories Ltd., Canada, using inductively coupled plasma-emission spectrometry (ICP-ES) for major elements and inductively coupled plasma-mass spectrometry (ICP-MS) for trace and rare earth elements (REE). Major oxide data were reported on a 0.2 g sample analyzed by ICP-ES following a lithium metaborate/tetraborate fusion and dilute nitric digestion. Loss on ignition (LOI) was determined by weight difference after ignition at 1000 °C. Average detection limit is 0.5 ppm for trace elements, 0.01 wt% for major oxides and 0.007–0.012 ppm for the REE. Therefore, three additional basalt samples of the Güzüngülü volcanics were performed at the Department of Geological Engineering at Pamukkale University, Turkey, using X-ray fluorescence spectrometry (XRF) for major and trace elements using the US Geological Survey (USGS) GEOL, GBW-7109 and GBW-7309 reference standards. The precision of these data is 0.5 ppm for heavy elements and 10 ppm for light elements. The major element data in Appendix C of Electronic Supplementary Material include water contents, but they have been recalculated on water-free basis for plotting in the classification diagrams.

Selected grains (sanidine, biotite) from each sample were chosen for laser $^{40}Ar/^{39}Ar$ single-crystal total fusion (SCTF) analysis and incremental heating analysis at Auburn University (USA) in the Auburn Noble Isotope Mass Analysis Laboratory (ANIMAL) which is equipped with a low-volume, high-sensitivity 10-cm-radius-sector mass spectrometer and automated sample extraction system (based on a CO_2 laser) for analysis of samples. Details of the analytical methods and data repositories are given in Appendix A of Electronic Supplementary Material, with a summary of the age data presented in Table 1.

Analyses of $^{87}Sr/^{86}Sr$ and $^{143}Nd/^{144}Nd$ isotope ratios of eight samples were carried out. The samples were not leached before analysis, as they do not contain evidence of alteration or secondary minerals. The Sr–Nd isotopic analyses were performed at University of North Carolina, Chapel Hill, USA, and at the Middle East Technical University Central Laboratory (METU, Ankara, Turkey). The

Table 1 Summary of single-crystal and step-heating ^{40}Ar–^{39}Ar dating and Sr and Nd isotopic analysis results of eight samples from the volcanic rocks in the Simav graben

Sample	Unit	Rock type	UTM coordinates	$^{40}Ar/^{39}Ar$ (plateau age) (Ma)	Single-crystal age (Ma)	$^{87}Sr/^{86}Sr$	$\pm 2\sigma$	$^{143}Nd/^{144}Nd$	$\pm 2\sigma$	$^{147}Sm/^{144}Nd$	$\pm 2\sigma$	$^{87}Sr/^{86}Sr_{(i)}$	$^{143}Nd/^{144}Nd_{(i)}$
D880	AV	Rhyolite	703409/4327035	19.81 ± 0.07 (Bt) 19.82 ± 0.07 (Bt) 19.20 ± 0.04 (Sa)		0.709698	10	0.512366	7	0.1005	7	0.708993	0.512353
D812	AV	Rhyolite	706808/4326818	18.04 ± 0.02 (Sa) 18.06 ± 0.02 (Sa)	18.04 ± 0.11 (Sa)	0.708323	9	0.512353	5	0.1143	8	0.707996	0.512341
D868	GV	Andesite	701729/4326674	–		0.708451	10	0.512377	6	0.1221	9	0.708267	0.512366
D822	GV	Andesite	713320/4328350	Did not define age		0.708140	8	0.512432	6	0.1197	9	0.708051	0.512421
D8257	GV	Basalt	695880/4312880	–	–	0.708248	4	0.512439	3			0.708223	0.512427
D8258	GV	Basaltic andesite	695980/4312750	–	–	0.708256	8	0.512453	3			0.708240	0.512441
D8118	ŞL	Lamproite	699680/4324941	15.56 ± 0.06 (Phl)	15.74 ± 0.06 (Phl)	0.708084	10	0.512455	7	0.1069	8	0.707759	0.512445
D916	IB	Basalt	693650/4317234	Did not define plateau (total gas age 16.33 ± 0.23 WR)		0.707396	10	0.512476	5	0.1066	8	0.707312	0.512466

AV Akdağ volcanics, *GV* Güzüngülü volcanics, *ŞL* Şaphanedağı lamproite, *IB* Inceğiz basalt, *Bt* biotite, *Sa* sanidine, *Phl* phlogopite, *WR* whole rocks

analyses at Chapel Hill were conducted using procedures a fully automated Micromass Sector 54 thermal ionization mass spectrometer (TIMS). $^{87}Sr/^{86}Sr$ analyses of strontium carbonate standard SRM 987 during this study yielded a value of 0.710245 ± 18 (2σ). At METU, the analyses were conducted using procedures similar to those described by Romer et al. (2001). During the study, NIST SRM 987 was measured as 0.710247 ± 10 ($n = 3$). Measurement of the Nd La Jolla standard gave a value of 0.511846 ± 5 ($n = 3$).

Geological setting and field relations of the magmatic rocks

The study area is located in the ~E–W-trending Pliocene–Quaternary Simav half-graben, which lies between the NE–SW-trending Demirci and Selendi basins in the south and NE–SW-trending Emet basin in the north (Fig. 1). The Neogene stratigraphy in the eastern part of the Simav half-graben is similar to those of the surrounding basins. The basement rocks of the Neogene volcano-sedimentary units in the area are represented by: (1) metamorphic rocks of the MCC and the Afyon zone and (2) ophiolitic mélange units of the İzmir-Ankara zone. These pre-Neogene units were intruded by the Lower Miocene Eğrigöz and Pınarbaşı granitoids. The Eğrigöz granitoid is a syn-extensional granitoid emplaced during the first-stage exhumation of the MCC (Işık et al. 2003). The granitoid yielded 19.0 ± 0.1 Ma hornblende and 20.2 ± 0.3–18.9 ± 0.1 Ma biotite Ar–Ar ages (Işık et al. 2004; Altunkaynak et al. 2012) and 20.7 ± 0.6–19.5 ± 0.3 U–Pb zircon ages (Ring and Collins 2005; Altunkaynak et al. 2012). The Pınarbaşı Granitoid is a small granitic intrusion cutting the limestones and mélange rocks of the İzmir–Ankara zone. Samples from the granite yielded 17.58 ± 0.03–17.67 ± 0.04 Ma biotite Ar–Ar ages (Semiz et al. 2010). The volcanic rocks in the region were emplaced synchronously with the deposition of the basin fill (Fig. 2a, b). The Neogene volcano-sedimentary units in the region were deposited coeval with the tectonic exhumation of the metamorphic rocks of the MCC (Ersoy et al. 2010a, 2011; Karaoğlu et al. 2010).

The Akdağ volcanics in the lower part of the sequence (in the Lower Miocene Hacıbekir Group) are composed of widely distributed pyroclastic rocks, dacitic-rhyolitic domes and massive lava flows. The pyroclastic rocks begin with white-colored pumice-rich tuffs with regular bedding planes, which are overlain by lithic-rich ignimbrites, which are overlain in turn by crystal-rich tuffs. The last products of the Akdağ volcanics are rhyolitic lava flows. Seyitoğlu et al. (1997) obtained 20.0 ± 0.6, 20.3 ± 0.6 and 17.6 ± 1.0 Ma (K–Ar) ages for these volcanics. In this study, 18.04 ± 0.02 and 19.82 ± 0.07 Ma Ar–Ar radiometric ages were obtained from the unit. These age data

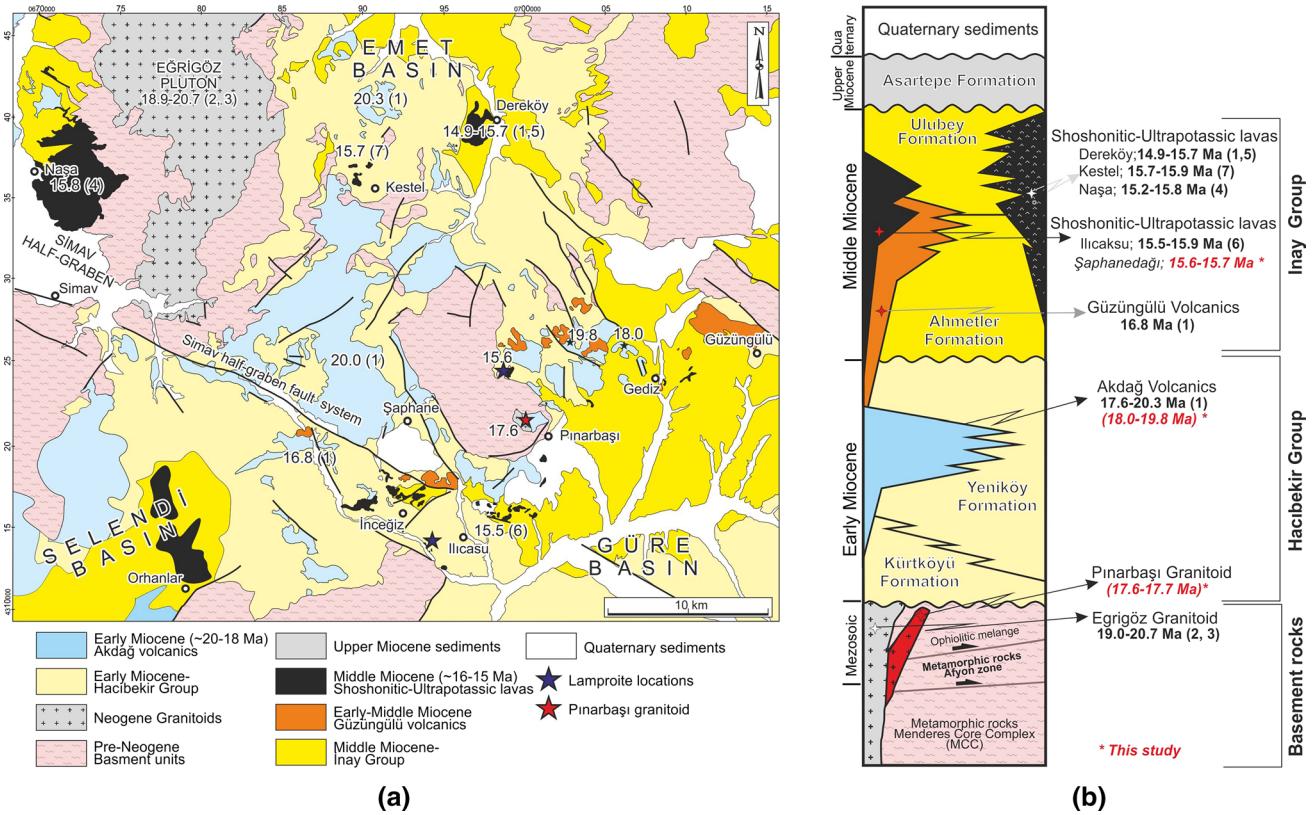

Fig. 2 Geological map (**a**) and stratigraphic columnar section (**b**) of the Simav Half-Graben (see Fig. 1 for location of the map). Age data from: (*1*) Seyitoglu et al. (1997), (*2*) Işık et al. (2004), (*3*) Altunkaynak et al. (2012), (*4*) Ercan et al. (1996), (*5*) Çoban et al. (2012), (*6*) Innocenti et al. (2005) and (*7*) Ersoy et al. (2012a)

demonstrate that the Akdağ volcanics developed during the Burdigalian (Early Miocene). On the basis of stratigraphic relations, correlative units of the Akdağ volcanics are also seen in the Demirci basin (Sevinçler volcanics; 19.06 ± 0.05–19.75 ± 0.05 Ma; Ersoy et al. 2012a) and in the Selendi basin (Eğreltidağ volcanics; 20.0 ± 0.2–18.9 ± 0.6 Ma; Seyitoğlu et al. 1997; Ersoy et al. 2010b).

The upper parts of the Neogene sequence (the Middle Miocene İnay group) are intercalated with the Güzüngülü volcanics, which are composed of andesitic lava flows, basaltic dykes and pyroclastic rocks. Seyitoğlu et al. (1997) obtained a 16.8 ± 0.7 Ma K–Ar age from an andesitic lava flow. Correlative units of the Güzüngülü volcanics are also seen in the Demirci basin (Asitepe volcanics; 17.58 ± 0.09 Ma; Ersoy et al. 2012a) and in the Selendi basin (Yağcıdağ volcanics; 16.61 ± 0.14–16.43 ± 0.32 Ma; Seyitoğlu et al. 1997; Purvis et al. 2005; Ersoy et al. 2008, 2012a).

The Middle Miocene sediments are also intercalated with locally developed small-volume lamproitic (Ilıcaksu and Şaphanedağı lamproites) and basaltic (İnceğiz basalt) lava flows in the study area (Fig. 2a). The Ilıcaksu lamproite yielded 15.87 ± 0.13–15.54 ± 0.06 Ma phlogopite Ar–Ar ages (Innocenti et al. 2005; Prelević et al. 2012). In this study, 15.56 ± 0.06 and 15.74 ± 0.06 Ma phlogopite Ar–Ar ages were obtained from the Şaphanedağı lamproite. The syn-sedimentary İnceğiz basalt conformably overlies the fluvio-lacustrine sedimentary rocks of the İnay group with peperitic contact relations, suggesting that these rocks are also Middle Miocene in age. Several mafic lava flows are also seen in the İnay group, including the Dereköy basalt (15.7 ± 0.4–14.9 ± 0.6 Ma; Seyitoğlu et al. 1997; Helvacı and Alonso 2000; Çoban et al. 2012) and Kestel volcanics (15.91 ± 0.07–15.73 ± 0.11 Ma; Ersoy et al. 2012a) to the south of the Emet basin, the Naşa basalt (15.2 ± 0.3–15.8 ± 0.3 Ma; Ercan et al. 1996) to the north of the Demirci basin, the Orhanlar basalt to the north of the Selendi basin, Kıran-Zahman basalts (15.50 ± 0.40 Ma; Seyitoğlu et al. 1997) in the Güre basin and the İnceğiz and Gediz basalts in the study area.

^{40}Ar–^{39}Ar geochronology

Ar–Ar age determinations were performed on samples from the Akdağ volcanics (samples D812 and D880),

Şaphanedağı lamproite (sample D8118) and İnceğiz basalts (sample D916). A summary of the ^{40}Ar–^{39}Ar age determinations of the volcanic rocks from this study is given in Table 1, and selected age spectra are illustrated in Fig. 3.

Sanidine phenocrysts from a rhyolitic lava sample of the Akdağ volcanics (sample D812) yielded age spectra that are almost ideally flat (concordant ages) (Fig. 3a, b). Similarly good plateau ages were obtained from a K-feldspar separate from another rhyolite lava sample (sample D880) of the from Akdağ volcanics and from biotite phenocrysts from the same sample (Fig. 3d–f). Laser $^{40}Ar/^{39}Ar$ analysis of one sample (D812) from the Akdağ volcanics yields single-crystal total fusion ages (Fig. 3c) that are in good agreement with the plateau ages. A phlogopite separate from the Şaphanedağı lamproite (sample D8118) gave a single-crystal age that is slightly older than the plateau age (Fig. 3g, h). In contrast, groundmass from a basalt sample of the İnceğiz basalts (sample D916) did not define plateau age (Fig. 3i), but yielded a total gas age of 16.33 ± 0.23. The U-shape of the spectrum suggests that excess argon and argon loss may be present.

Overall, the age data indicate that the volcanism in the study area occurred during the Early and Middle Miocene and is similar in age to volcanism described from the Demirci, Selendi and Uşak-Güre basins (Ersoy et al. 2008, 2011, 2012a; Karaoğlu et al. 2010).

Petrography and mineral chemistry of the magmatic rocks

Field occurrences, petrographic features and geochemical data of the volcanic rocks in the study area indicate that they can be grouped as: (1a) Lower Miocene Akdağ volcanics and Pınarbaşı granitoid, (1b) Lower–Middle Miocene Güzüngülü volcanics and (2) Middle Miocene mafic lavas with shoshonitic–ultrapotassic geochemistry. Textural and mineralogical characteristics of representative samples from these groups are summarized in Table 2, and mineral compositions of representative samples are reported in Appendix B of Electronic Supplementary Material.

The Akdağ volcanics are composed of mainly rhyolitic and rarely dacitic lava flows and related pyroclastic rocks. The rhyolites contain quartz, sanidine, plagioclase ($An_{30–39}$), biotite and magnetite phenocrysts, and rarely hornblende, apatite and zircon (Figs. 4, 5). The feldspar microlites are mainly sanidine ($Or_{74–77}$). Plagioclase shows complex zoning and spongy-cellular (sieve) textures and oscillatory zoning (Fig. 4a, b). Some plagioclase phenocrysts include clinopyroxene, biotite, apatite and opaque inclusions. Biotites have low Mg# (46.6–50.8) (Fig. 5d). The Pınarbaşı granitoid contains plagioclase, K-feldspar, quartz, biotite and hornblende, with accessory apatite, sphene, zircon, magnetite and muscovite, and based on its modal and geochemical classification it is composed of granite, granodiorite and quartz monzonite (Table 3).

The Güzüngülü volcanics are composed of lava flows and dykes with a wide range of compositions from basalt to dacite and related pyroclastic rocks. The samples have mainly porphyric, hyalopilitic, hypocrystalline, vitrophyric and rarely perlitic textures. The basalts consist of plagioclase ($An_{33–41}$ in the rim and $An_{67–70}$ in the core), clinopyroxene ($En_{46–50}Wo_{40–44}$), orthopyroxene and Fe–Ti oxide (Figs. 4, 5). The andesitic to trachyandesitic lava flows generally share similar petrographic characteristics and consist of mainly plagioclase ($An_{46–89}$), clinopyroxene ($En_{43–45}Wo_{41–44}$), orthopyroxene ($En_{64–76}Wo_{0.5–3.4}$), hornblende (Mg# 76–83) with minor phases of biotite (Mg# 68–82) and Fe–Ti oxides in glassy matrix. The dacitic lavas contain quartz, plagioclase ($An_{40–87}$), biotite (Mg# 55–65), and rarely hornblende (Mg# 65–82), clinopyroxene ($En_{42–46}Wo_{41–44}$) and sanidine. Plagioclase from all the samples shows complex zoning and spongy-cellular (sieve) textures, with rare reversely zoned phenocrysts. Some biotites are rimmed by Fe–Ti oxide grains.

The shoshonitic–ultrapotassic rocks (the Dereköy, Eskigediz and Inceğiz basalts, the Ilıcaksu and Şaphanedağı lamproites and the Kestel volcanics) display similar mineral assemblages of clinopyroxene, olivine, rarely phlogopite (İnceğiz basalt), plagioclase ($An_{72–80}$ in the Dereköy basalts and Kestel volcanics), and opaque minerals. The samples show glomeroporphyric, porphyritic, hyalopilitic, intersertal, pilotaxitic textures. Clinopyroxene, olivine and opaque mineral phenocrysts are enclosed within a glassy or fine-grained groundmass consisting dispersed microlites of plagioclase, clinopyroxene and opaque minerals. Clinopyroxene is ubiquitous in the basalts and dominates the phenocryst assemblage, with euhedral to subhedral, sometime rounded shapes that are weakly zoned and often have a sieve-textured (Fig. 4c). Clinopyroxene crystals in these rocks have variable Ca, Ti and Al contents (Appendix B of Electronic Supplementary Material), but they all lie between $Wo_{39–47}En_{40–50}$ and are classified as diopside and augite (Fig. 5b). Diopside and augite can be present in the same rock, both as uniform and zoned crystals. Zoned clinopyroxene shows increasing Fe and decreasing Ca from core to rim (Fig. 4d).

Unzoned subhedral olivine is abundant in the İnceğiz basalt. Fo contents of the olivine from İnceğiz basalt range from 76 to 80, and the olivine contains Cr spinel inclusions (Fig. 4e). Some grains show normal zoning. Phlogopite is Mg-rich, and Mg contents increase from rim to core (Fig. 4f). The Fe–Ti oxides in the mafic volcanic rocks include Ti-magnetite and magnetite, along with ilmenite in those with transitional affinity (Bacon and Hirschmann 1988; Appendix B of Electronic Supplementary Material, Fig. 4e).

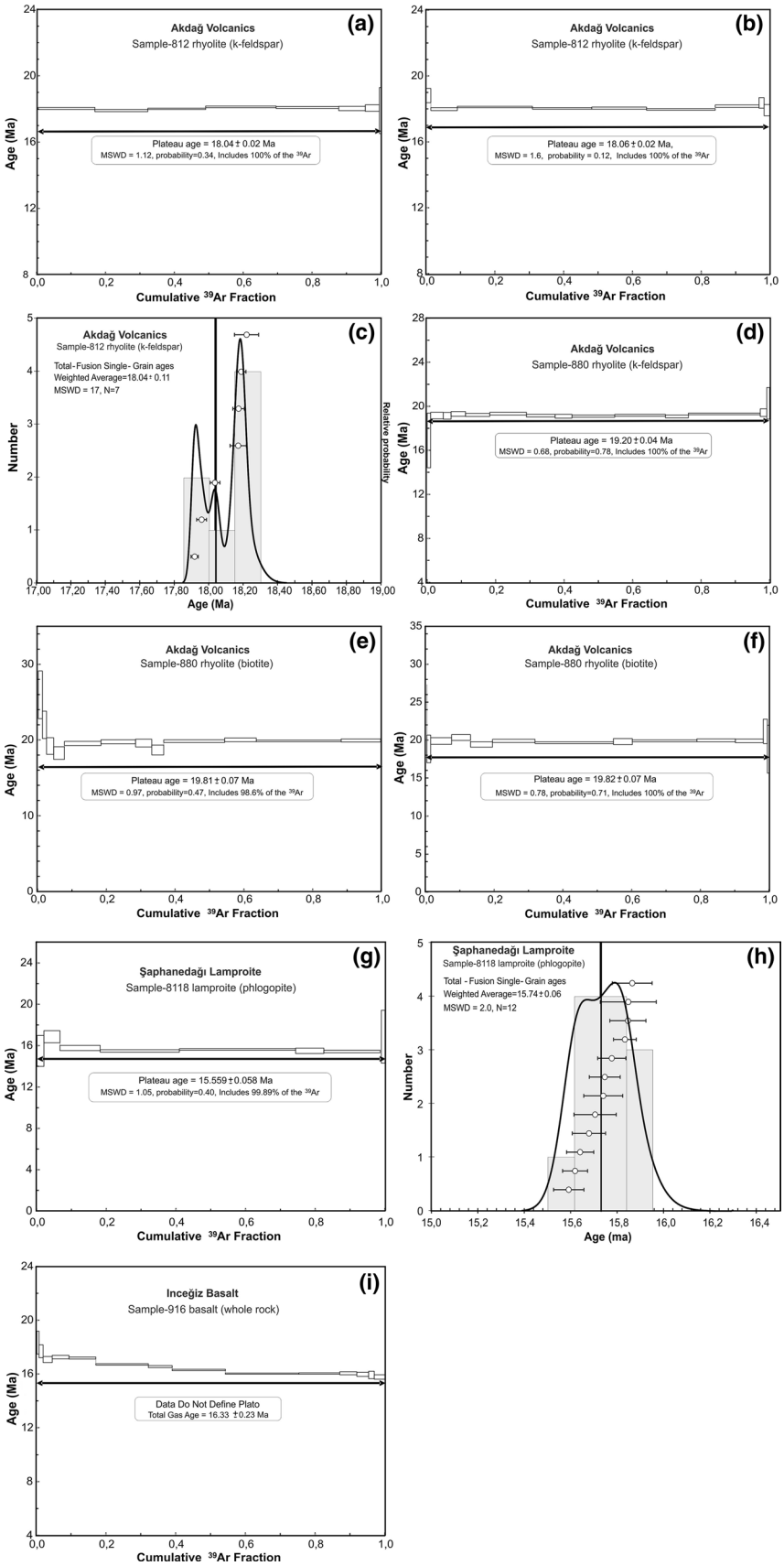

Fig. 3 **a–i** Apparent age spectra for the dated volcanic rocks in this study

Table 2 Petrographic compositions of the volcanic rocks in the Simav graben

Formations	Rock type	Texture	Q	Ol	Cpx	Opx	Plg	Snd	Hbl	Bio	Phl	Mg	Il	Ap
Akdağ	Rhyolite	Hyalopilitic, vitrophyric	+				+	+	ǂ	+		+		+
Güzüngülü	Dacite	Hypocrystalline, hyalopilitic, vitrophyric, rarely perlitic	+		+	ǂ	+	ǂ	+	+	ǂ	+		+
Güzüngülü	Andesite	Hyalopilitic, vitrophyric, glomeroporphyric			+	+	+		+	ǂ		+		
Güzüngülü	Trachyandesite	Pilotaxitic, hyalopilitic, glomeroporphyric			+	+	+		+	ǂ		+		
Güzüngülü	Basalt	Hypocrystalline, hyalopilitic			+		+					+		
Dereköy	Basalt	Porphyric, rarely hyalopilitic		ǂ	+						ǂ	+	ǂ	
Inceğiz	Olivine Basalt	Pilotaxitic, rarely hyalopilitic		+	+		+				+	+	+	
Naşa	Basalt	Porphyric, pilotaxitic, rarely hyalopilitic		ǂ	+		+				+	+		
Eskigediz	Basalt	Microlitic, hypocrystalline			+		+	+			+	+	ǂ	
Kestel	Basalt	Hypocrystalline, glomeroporphyric			+		+	+			+	+	+	
Ilıcaksu	Lamproite	Poikilitic		+	+			+			+	+	+	+
Şaphanedağı	Lamproite	Poikilitic			+			+			+	+	+	+

The Ilıcaksu lamproite consists of olivine, phlogopite, clinopyroxene (diopside–augite), sanidine and apatite, with accessory magnetite and ilmenite. The samples contain both phenocrysts and xenocrysts hosting Cr spinels. The olivine xenocrysts can be considered as mantle olivines on the basis of their CaO contents (Fig. 5f). The xenocrysts are zoned and Fo rich (up to 92). NiO contents are <0.8 (wt%) in the core and show low Fo (up to 82) and NiO (<0.25 wt%) in the rim. The phlogopite has low Mg# and TiO_2 (up to 4 wt%) and opacite rims with high TiO_2 (up to 9 wt%). The diopside and augites have typical lamproitic clinopyroxene character, with high Mg# and low TiO_2 and Na_2O contents. Apatite occurs as prismatic crystals, needle-like microphenocrysts as well as inclusions in phlogopite (Semiz 2010). The Şaphanedağı lamproite contains zoned phlogopite (Mg# 70.3–90.1) and clinopyroxene (diopsidic augite). The matrix of the lava flows also includes sanidine. These rocks contain apatite, ilmenite and magnetite as accessory phases. Clinopyroxene is generally zoned. The micas are present as Mg-rich biotite (low MgO, 17.1 %) in the rims and phlogopite (high MgO, 20.2 %) in the core (Fig. 5d).

Temperature and pressure conditions of the volcanic rocks were calculated from pyroxene, plagioclase and olivine–Cr spinel minerals using the constraints described by Nimis (1995), Putirka et al. (2003) and Putirka (2008) and are listed in Table 4. The temperature variations in clinopyroxene do not vary significantly from core to rim in the volcanic rocks.

Major and trace elements

Samples of the Pınarbaşı granitoid are classified as HKCA granite, granodiorite and quartz monzonite with a weak peraluminous and I-type geochemical affinity. These rocks geochemically resemble the Lower Miocene Eğrigöz granitoid. The Lower Miocene Akdağ volcanics (SiO_2 = 67.5–74.2; MgO = 0.3–1.1 wt%) are classified as rhyolite with a dominant HKCA to shoshonitic affinity according to their K_2O contents which highly varies in a restricted SiO_2 range (~70–75 wt%) (Fig. 6a, b). These rocks show a peraluminous character and are thus geochemically well correlated with the other Lower Miocene dacitic to rhyolitic volcanic units and the granitoids in the region.

Samples of the Güzüngülü volcanics have lower silica and higher MgO contents (SiO_2 = 48.7–64.0; MgO = 0.5–8.3 wt%) with respect to the Lower Miocene volcanic and plutonic rocks in the region, and are mainly classified as HKCA basalt, basaltic andesite, andesite, latite and dacite. The andesitic to dacitic rocks of the Güzüngülü volcanics are geochemically well correlated with the other Lower–Middle Miocene volcanic units in the region (Fig. 6).

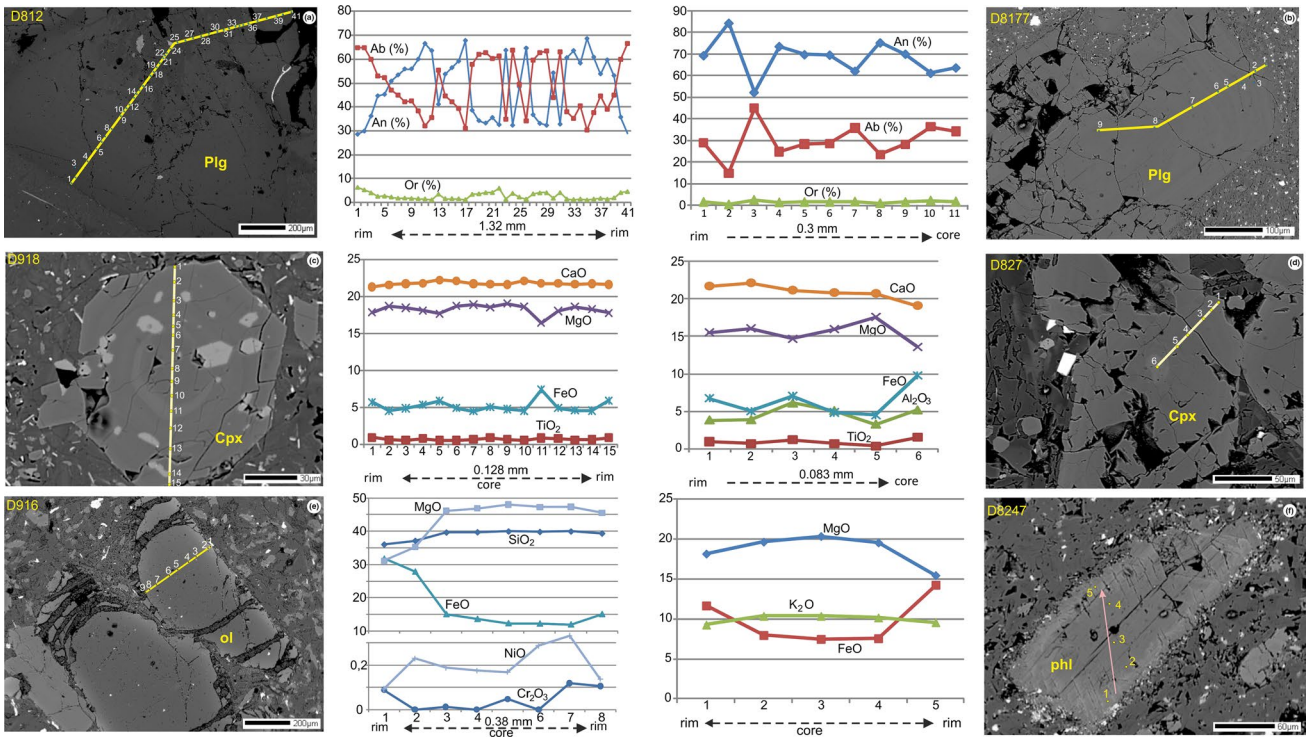

Fig. 4 Typical zoning patterns of selected phenocrysts from the volcanic rocks. **a** Oscillatory plagioclase in a rhyolite from the Akdağ volcanics (sample D812), **b** plagioclase phenocryst in a trachyandesite from the Güzüngülü volcanics (sample D8177), **c** clinopyroxene phenocryst in the Inceğiz basalt (sample D918), **d** clinopyroxene phenocryst in the Eskigediz basalt (sample D827), **e** olivine phenocryst in the Inceğiz basalt (sample D916), **f** mica phenocryst in the Kestel volcanics (sample D8247). *Pl* plagioclase, *cpx* clinopyroxene, *ol* olivine, *phl* phlogopite

Figure 6d shows that the products of Lower–Middle Miocene andesitic volcanism differ from the Early Miocene rhyolitic volcanic rocks in respect of their alumina saturation, with the former characterized by dominantly metaluminous affinity, while the latter show a dominant peraluminous character.

The Middle Miocene mafic volcanic rocks in the region (SiO_2 = 50.3–59.2; MgO = 1.8–12.5 wt%; Mg# = 36.0–77.9) plot in the shoshonite/latite fields with potassic alkaline compositions (Fig. 6a). Excepting for the Eskigediz and Kestel basalts, which have either ultrapotassic or shoshonitic character, all the other units show a strong ultrapotassic character according to criteria of Foley et al. (1987). The Middle Miocene shoshonitic–ultrapotassic (SHO–UK) rocks with high-MgO contents geochemically resemble other orogenic ultrapotassic rocks along the Alpine–Himalayan system (from Spain, Italy, Serbo-Macedonia and the Afyon region in Turkey) (Akal 2008; Altherr et al. 2004; Benito et al. 1999; Duggen et al. 2005; Prelević et al. 2005, 2008, 2012, 2013; Çoban and Flower 2006; Gao et al. 2007; Yanev et al. 2008; Conticelli et al. 2009; Tommasini et al. 2011; Semiz et al. 2012; Prelević et al. 2015) (Fig. 7). Overall, all these volcanic rocks, together with the other Middle Miocene mafic volcanic units in the region with similar geochemical features, are grouped as SHO–UK in the following discussion.

The magmatic rocks in the area contain both high-SiO_2 (andesite–rhyolite) and high-MgO (basaltic and shoshonitic–ultrapotassic mafic) series. Therefore, in order to monitor the major and trace element variations of the rock series, the data are plotted against both SiO_2 and MgO contents as differentiation indices on Fig. 8. All rocks show decreasing trends in Fe_2O_3 and CaO as their SiO_2 contents increase and MgO contents decrease. The SHO–UK rocks show highly variable K_2O contents. The Al_2O_3 contents first increase and then decrease from the most primitive to most evolved samples for all rock groups. In general, TiO_2 compositions decrease with increasing differentiation, but the shoshonitic and ultrapotassic rocks show more variable relationships. Except for Zr, Rb and Ba, the trace element variations in the all volcanic rock groups display clear negative correlations with increasing SiO_2 contents and positive correlations with decreasing MgO contents.

Overall, the trace and major element data indicate that the Akdağ and Güzüngülü volcanics evolved from a primitive melt that may be most closely represented by the lowest SiO_2-highest MgO sample of the Güzüngülü volcanics (sample D8257). Note that the geochemical composition of

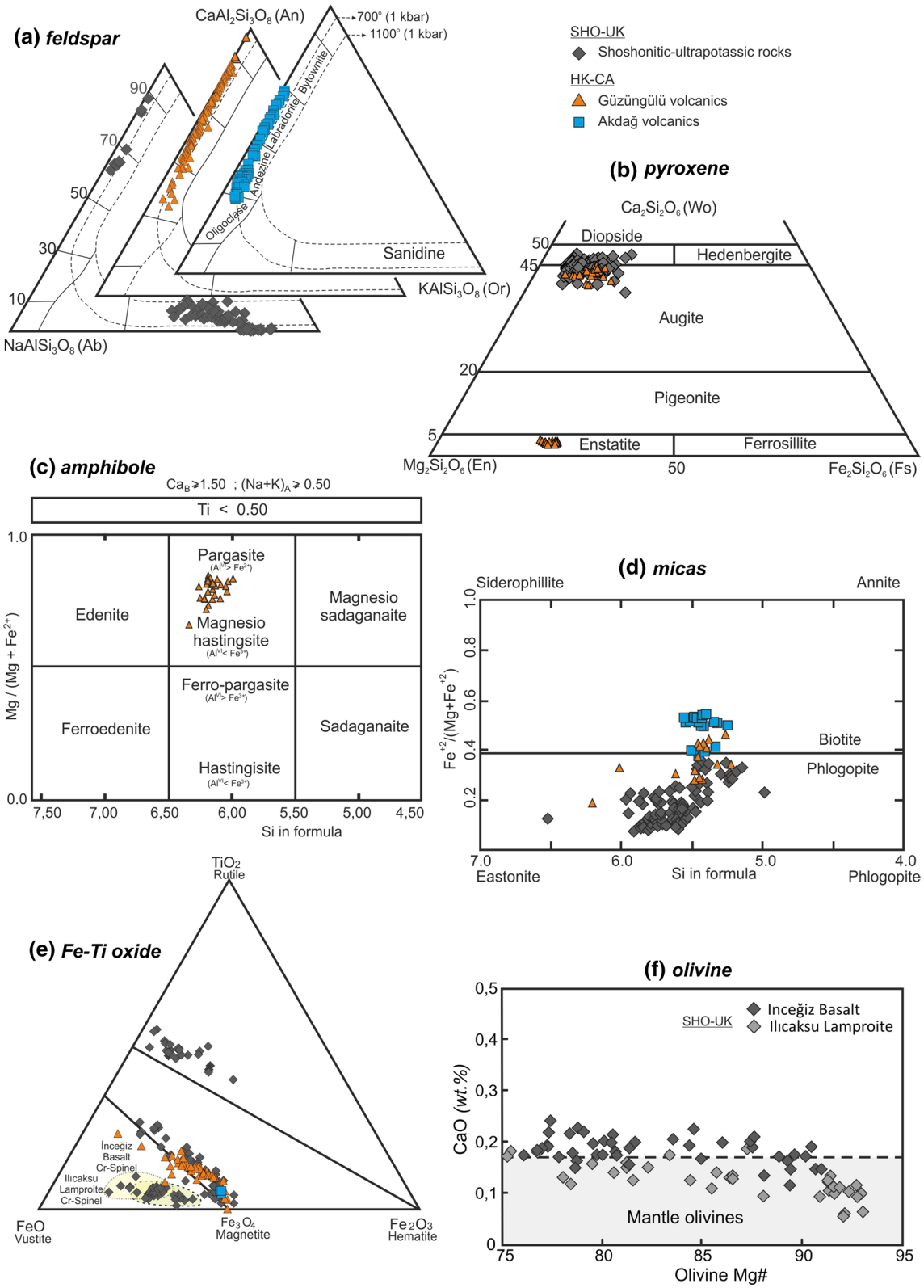

Fig. 5 Phenocryst classification diagrams of the volcanic rocks from the Simav graben. **a** Ternary Ab–Or–An classification diagram of feldspars (Deer et al. 1966). *Dashed curves* represent isotherms of Fuhrman and Lindsley (1988), **b** pyroxene (enstatite–ferrosilite–diopside–hedenbergite) classification diagram (Morimoto 1988), **c** hornblende classification diagram (Leake et al. 1997), **d** mica classification diagram (Rieder et al. 1999), **e** ternary rutile–wustite–hematite diagram of Fe–Ti oxide, **f** Fo (forsterite = 100 Mg/(Mg + Fe), where Mg and Fe represent molar proportions) versus wt% CaO plot of olivine phenocrysts (Thompson and Gibson 2000)

Table 3 Least squares major element modeling results for HKCA rocks (using PETROGRAPH software of Petrelli et al. 2005)

	D8257	D814	D828	Cpx	Amp	Plg	Snd	Mag
100 % normalized oxide compositions (wt%)								
SiO_2	52.62	61.56	65.38	51.75	42.97	51.83	61.75	2.48
Al_2O_3	14.20	18.84	16.32	2.88	12.13	30.35	23.35	1.98
FeO_{tot}	8.27	3.95	4.75	9.13	11.63	0.56	0.21	88.08
MgO	8.39	1.72	1.04	18.12	14.29	0.03		2.01
CaO	11.11	5.49	4.51	16.93	12.16	13.23	4.15	0.17
Na_2O	2.61	3.37	3.42	0.26	2.17	3.56	4.83	
K_2O	1.53	3.87	3.61	0.02	1.02	0.34	5.66	
TiO_2	0.89	0.77	0.69	0.62	3.40	0.04	0.03	4.45
P_2O_5	0.22	0.33	0.21					
MnO	0.16	0.09	0.05	0.28	0.22	0.05	0.04	0.84

	Starting magma	Final magma	Ol (%)	Cpx (%)	Pl (%)	Sa (%)	Amp (%)	Mag (%)	Bio (%)	Cryst.%	Σr^2
First stage	D8257	D814	0.1	48.1	24.8		23.0	4.0		64.4	0.272
Second stage	D814	D828			25.2	55.5	10.3		9.0	37.5	0.116

The compositions of the minerals used in the calculations are from average results of microprobe results

Table 4 Temperature and pressure conditions of the volcanic rocks were calculated from pyroxene, plagioclase and olivine–Cr spinel minerals using the constraints described by Nimis (1995), Putirka et al. (2003) and Putirka (2008)

Rock type	Mineral	Temperature (°C)	Pressure (kbar)
Calculated pressure–temperature conditions for the volcanic rocks in the study area			
Akdağ volcanics	Plagioclase	930	
Güzüngülü dacite	Clinopyroxene	975	6.2
Güzüngülü trachyandesite	Clinopyroxene	1051	7.0
Güzüngülü andesite	Clinopyroxene	1117	6.0
Güzüngülü basalt	Clinopyroxene	1232	7.5
Kestel basalt	Clinopyroxene	1066	8.7
Inceğiz basalt	Clinopyroxene	1191	7.6
Eskigediz basalt	Clinopyroxene	1189	8.4
Dereköy basalt	Clinopyroxene	1149	4.9
Şaphanedağı lamproite	Clinopyroxene	1097	10.3
Ilıcaksu lamproite	Olivine	1257	7.1

this sample differs significantly from those of the SHO–UK rocks with similar MgO contents (Fig. 8). In particular, for a given MgO content, the most primitive samples of the Güzüngülü volcanics have higher Fe_2O_3, CaO, Al_2O_3, Sc, Sr, but lower K_2O, TiO_2, Ni, Rb, Zr and REE contents than the SHO–UK samples.

Trace element compositions of the magmatic units are also shown in primitive mantle (PM)-normalized multi-element spider diagrams (Fig. 9). All the rocks in the study area show enrichments in large ion lithophiles and light rare earth elements (LILE and LREE, respectively), and relative depletions in high-field-strength elements (HFSE). Samples of the Pınarbaşı granitoid are similar to those of the Eğrigöz granitoid, but the latter have distinctly higher Sr levels (Fig. 9a). The Akdağ volcanics have similar trace element patterns to those of the other Lower Miocene dacitic to rhyolitic volcanic rocks in the region (Fig. 9b), and the trace element abundances and patterns of the Lower Miocene plutons and volcanic rocks are also comparable.

Similarly, the Güzüngülü volcanics show similar trace element patterns to those of the other andesitic to dacitic rocks in the region, but the latter group has distinctly higher Zr and Hf and lower Sr abundances. Sample D8257, the most primitive sample of the Güzüngülü volcanics, has the lowest trace elements abundances of all the rock samples in this group (Fig. 9c). The SHO–UK samples in the region have generally similar trace element patterns to those of the other rock groups, although they have slightly higher abundances of most elements. Among this group, the ultrapotassic rocks have higher Zr and Hf levels than the shoshonitic rocks (Fig. 9d).

Overall, the geochemical data from the magmatic rock groups suggest the following: (1) the HKCA and dominantly peraluminous rhyolitic (and dacitic) volcanics and granitic plutons were emplaced with similar geochemical features during the Lower Miocene; (2) two distinct magma lineages occurred during the late Lower–Middle

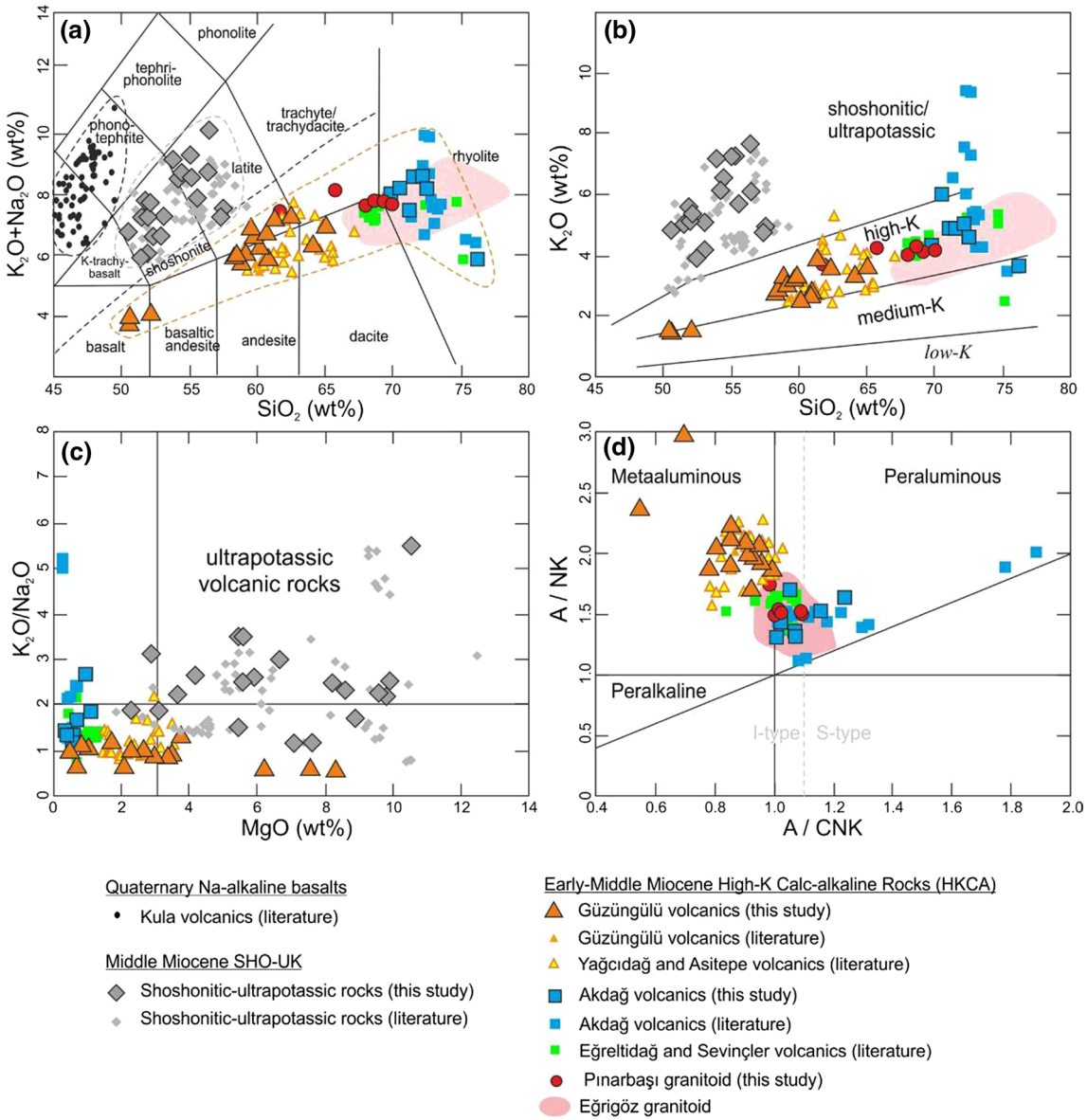

Fig. 6 Classification and discrimination diagrams for the magmatic units in the region. **a**, **b** Total alkali ($K_2O + Na_2O$) versus SiO_2 (wt%) (TAS) and K_2O versus SiO_2 (wt%) diagrams with IUGS fields (LeMaitre 2002), **c** K_2O/Na_2O versus MgO (wt%) diagram to discriminate the ultrapotassic rocks (after Foley et al. 1987), **d** the molar $Al_2O_3/Na_2O + K_2O$ (A/NK) versus $Al_2O_3/CaO + Na_2O + K_2O$ (A/CNK) (aluminum saturation index) diagram (Maniar and Piccoli 1989). Data are recalculated on anhydrous basis. The literature data are from Seyitoğlu et al. (1997), Innocenti et al. (2005), Karaoğlu et al. (2010), Ersoy et al. (2008, 2010a, b, 2012a), Çoban et al. (2012) and Prelević et al. (2012)

Miocene, producing (a) mainly HKCA volcanics and (b) high-MgO shoshonitic to ultrapotassic (SHO–UK) volcanics (including lamproites); (3) HKCA basaltic to dacitic volcanics likely evolved from a primitive magma composition that is best represented by the most basic sample of the Güzüngülü volcanics (i.e., sample D8257); and (4) the variable trace element contents of the SHO–UK samples for a given MgO content are comparable with other ultrapotassic volcanic rocks from the Alpine-Himalayan orogenic system, which are generally referred as orogenic ultrapotassic rocks (Benito et al. 1999; Altherr et al. 2004; Duggen et al. 2005; Prelević et al. 2005, 2008, 2012, 2013; Ersoy and Helvacı 2007; Conticelli et al. 2009; Tommasini et al. 2011; Semiz et al. 2012; Ozpinar et al. 2013).

Sr–Nd isotopes

The Sr–Nd isotopic data obtained in this study (Table 1) are compared with published data from the surrounding regions

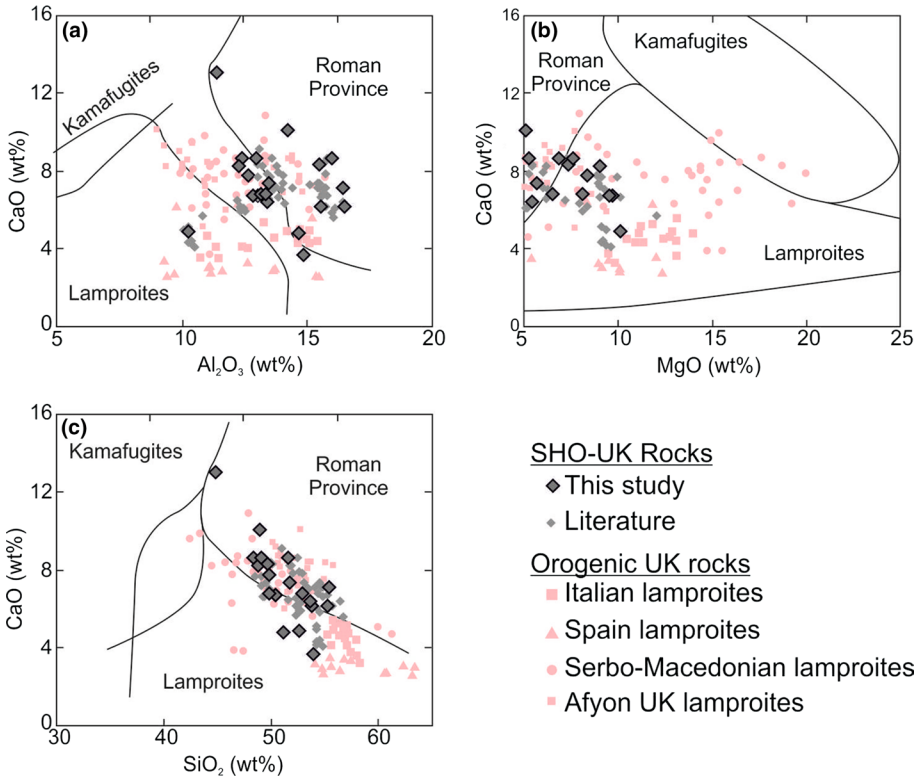

Fig. 7 **a–c** Classification diagrams for the high-MgO shoshonitic–ultrapotassic rocks in the region [adapted from Foley et al. (1987)]. Ultrapotassic lamproites from Italy, Spain, Serbia-Macedonia and Afyon (Turkey) are also shown for comparison. *Data source*: Benito et al. (1999), Altherr et al. (2004), Duggen et al. (2005), Prelević et al. (2005, 2008, 2012), Çoban and Flower (2006), Akal (2008), Conticelli et al. (2009), Yanev et al. (2008)

(Appendix C of Electronic Supplementary Material) in Fig. 10. These plots also include data from the post-collisional magmatic rocks of the Northwest Anatolian Eocene magmatics (NAEM) (Kürkçüoğlu et al. 2008; Chakrabarti et al. 2012; Altunkaynak et al. 2012; Gülmez et al. 2012) and from the Pliocene–Quaternary SAVA (Zellmer et al. 2000; Buettner et al. 2005; Bailey et al. 2009) for regional comparison.

The initial $^{87}Sr/^{86}Sr$ ratios of even the most primitive samples in the study area (highest MgO) are ~0.707–0.708, and the $^{87}Sr/^{86}Sr_{(i)}$ ratios of the evolved rocks of the HKCA series similarly vary in the range 0.708–0.710. Similarly, the $^{143}Nd/^{144}Nd_{(i)}$ values of the primitive samples also yield apparently continental crustal signatures in the range 0.5124–0.5125. Although there are wide Sr–Nd isotope ranges in the SHO–UK (with high MgO) samples and the HKCA basalt to rhyolite series, their Sr–Nd isotope ratios largely overlap (Fig. 10a). All the rock types in the study area plot on the lower-right quadrant of the $^{87}Sr/^{86}Sr_{(i)}$–$^{143}Nd/^{144}Nd_{(i)}$ diagram, and are thus distinct from the basaltic to granitic rocks of the NAEM and the basaltic to rhyolitic rocks of the SAVA (Fig. 10a).

The $^{87}Sr/^{86}Sr_{(i)}$ ratios of the volcanic rocks are plotted against their SiO_2 and MgO (wt%) contents (Fig. 10b, c). Although there may be some subtle relationships between the $^{87}Sr/^{86}Sr_{(i)}$ values and SiO_2 and MgO contents of the SHO–UK and HKCA samples, similar $^{87}Sr/^{86}Sr_{(i)}$ ratios are seen over a wide range of SiO_2 and MgO. The $^{87}Sr/^{86}Sr_{(i)}$–SiO_2 and $^{87}Sr/^{86}Sr_{(i)}$–MgO systematics of the rock groups in this study are, however, clearly distinct from the NAEM and SAVA groups. The low-SiO_2 and high-MgO samples of both the SAVA and NAEM groups have lower $^{87}Sr/^{86}Sr_{(i)}$ compositions (and also higher $^{143}Nd/^{144}Nd_{(i)}$ values, not shown) with respect to the most primitive samples of the SHO–UK and HKCA rocks in this study, and this difference is also seen in the most evolved samples (with higher SiO_2 and lower MgO contents). This observation supports the hypothesis (Ersoy and Palmer 2013) that the SHO–UK and HKCA rocks considered in this study, and elsewhere in the region, were derived from distinct (high $^{87}Sr/^{86}Sr$) mantle sources relative to the post-collisional rocks of the NAEM and volcanic arc rocks of the SAVA.

Discussion

The distinct geochemical trends observed in the HKCA rock groups likely resulted from different petrogenetic processes during their genesis, depending on: (1) melting parameters of their source rocks, such as starting composition and degree of melting, (2) depth of the magma chambers, (3) fractionating mineral assemblages, (4) possible mixing processes with distinct magma types and (5) difference in the nature of assimilated country rocks. Similar factors may also have influenced the genesis of the SHO–UK rocks as they also show variable trace element contents for a given MgO content, and variable trends in certain

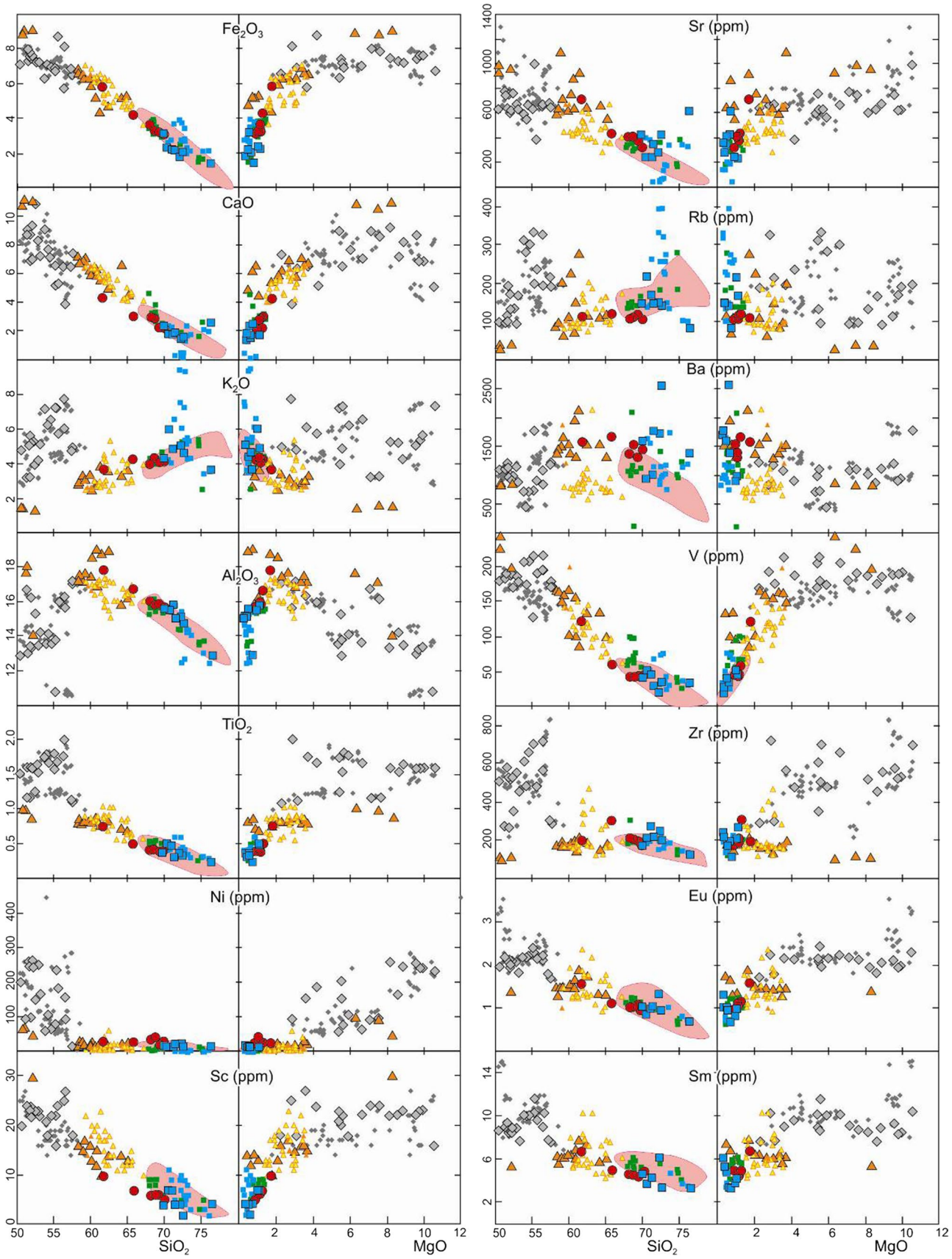

Fig. 8 SiO_2- and MgO-dependent major and trace element variation diagrams for the magmatic rock suites (*symbols* as in Fig. 6)

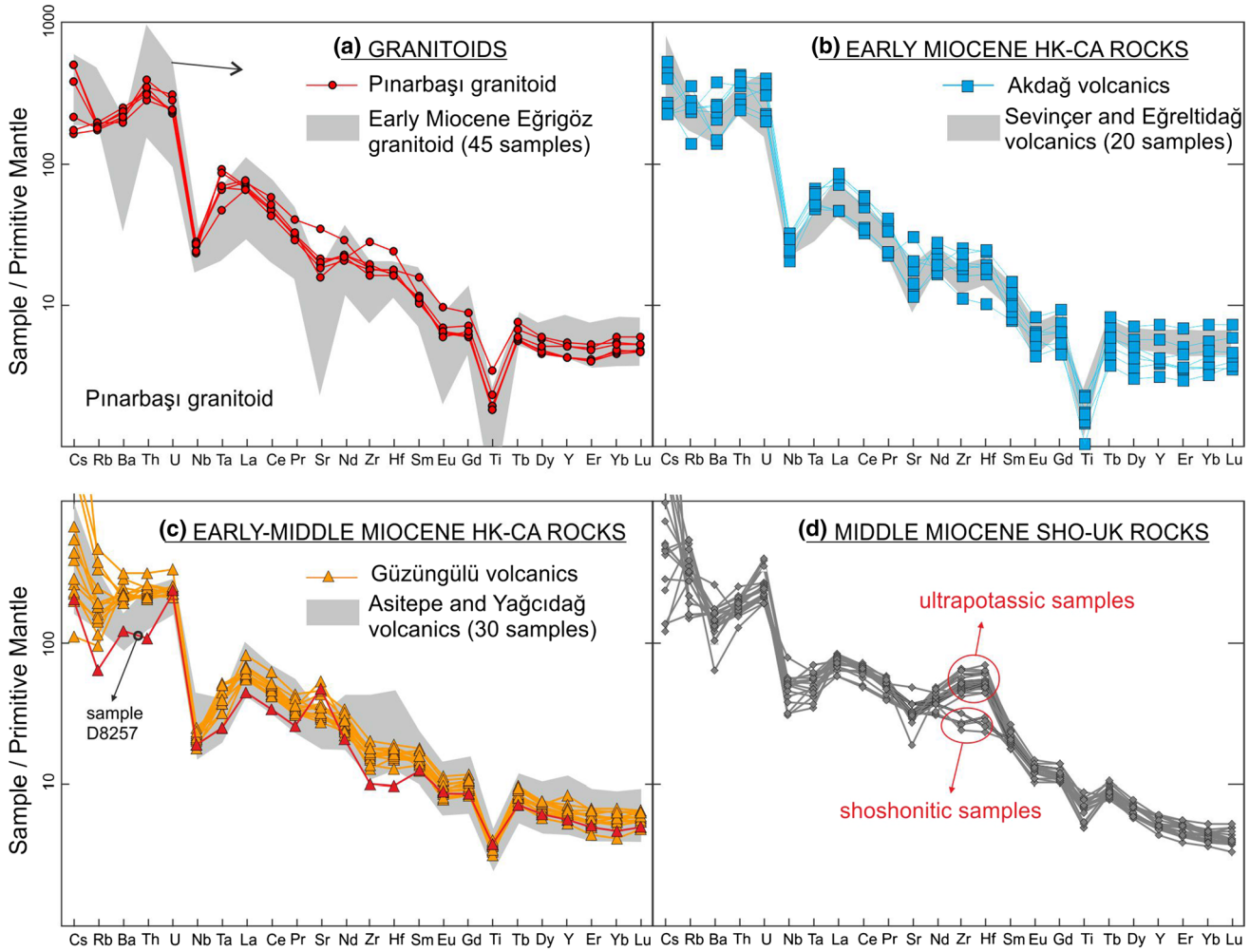

Fig. 9 Primitive mantle-normalized trace element patterns for magmatic rocks in the study area. Normalizing values from Palme and O'Neill (2004)

elements, such as TiO_2, K_2O, Zr and compatible trace elements. The effects of these processes will be discussed below.

Fractional crystallization

The major and trace element variation diagrams for the HKCA samples (Fig. 8) indicate that they have undergone varying degrees of fractional crystallization. Decreasing MgO, Fe_2O_3, CaO, Ni, V and Sc contents of the low- to medium-silica rocks (SiO_2 ~50 to ~62 wt%) are indicative of crystallization of pyroxenes (plus Fe–Ti oxides) and possibly olivine with subsidiary plagioclase during differentiation, and this hypothesis is supported by the observation of abundant clinopyroxene and Fe–Ti oxides in basaltic samples of the Güzüngülü volcanics of the HKCA group.

The more evolved rocks of the HKCA group, andesites to dacites, contain feldspars, hornblende and minor amount of pyroxenes, biotite and Fe–Ti oxides, so that crystallization of these minerals accounts for their decreasing MgO, Fe_2O_3, CaO, Na_2O, Al_2O_3, TiO_2, V and Eu contents with increasing SiO_2. The sharp decreases in MgO, Fe_2O_3, CaO, V and Sc likely result from fractionation of clinopyroxene and Fe–Ti oxides, while the absence of concomitant decreases in Rb contents indicate that the biotite was not involved (or was a minor phase) during fractionation. The slight decreases in Sm are compatible with the presence of amphibole in fractionation processes. K-feldspar fractionation can also be inferred for the dacitic to rhyolitic samples of the Early Miocene Akdağ volcanics, as indicated by decreasing K_2O contents of the high-silica samples.

The geochemical fractionation trends of the HKCA samples discussed above indicate that two distinct assemblages were fractionated during differentiation of the low- to high-SiO_2 rocks: clinopyroxene (cpx)-dominated [clinopyroxene + olivine + plagioclase and Fe–Ti

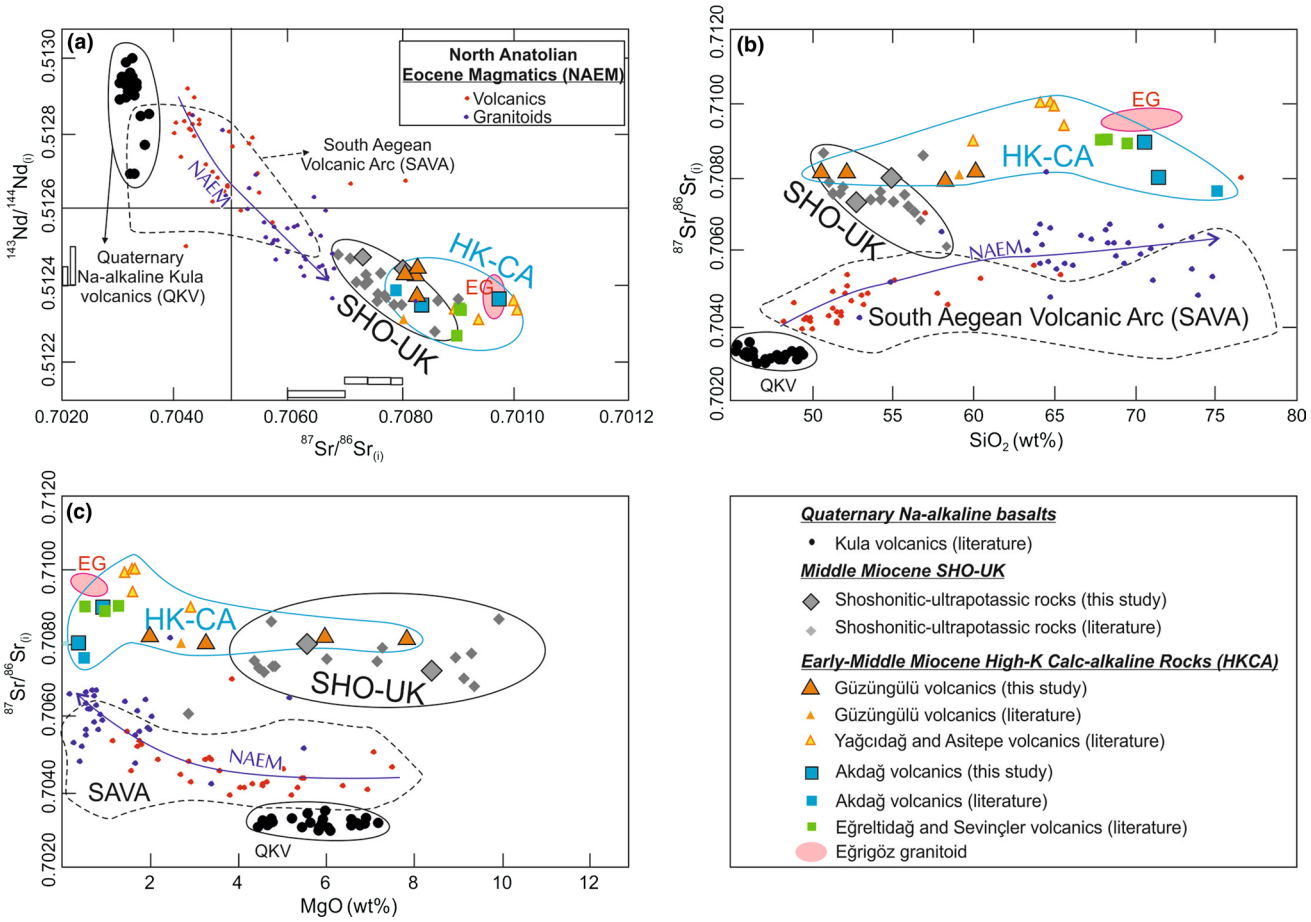

Fig. 10 Whole-rock Sr and Nd isotopic systematics of the volcanic rocks

oxides] and feldspar-dominated [plagioclase + clinopyroxene + sanidine + amphibole + minor biotite and Fe–Ti oxides]. Mass balance calculations have been performed (using PETROGRAPH software of Petrelli et al. 2005 and the partition coefficients of Ersoy et al. 2010b) based on two stages of fractionation, in which the samples D8257 (starting composition), D814 (mildly evolved composition) and D828 (final rhyolitic composition) from the Güzüngülü volcanics are used to constrain the calculations. The Akdağ volcanics were not included in these models because this phase of volcanism represents the older pulse of magmatic activity in the region. The results of the mass balance calculations show that 64.4 % fractionation of an assemblage composed of olivine (0.1 %) + clinopyroxene (48.0 %) + plagioclase (24.6 %) + amphibole (23.4 %) + magnetite (4.0 %) ($\Sigma r^2 = 0.27$) best reproduces the first stage of cpx-dominated fractionation (from sample D8257 to sample D814). While the second stage (from sample D814 to D828) is best replicated by 37.5 % fractionation of an assemblage of plagioclase (25.2 %) + sanidine (55.5 %) + amphibole (10.3 %) + biotite (9.0 %) ($\Sigma r^2 = 0.12$) (Table 3).

While not included in these models, the Akdağ volcanics appear to lie on an extended differentiation trend (to higher SiO_2 and lower MgO) of the Güzüngülü volcanics (Fig. 8). Hence, it appears likely that the dacite to rhyolites of the Akdağ volcanics originated from magmas which had similar initial compositions to the Middle Miocene HKCA samples and that the fractionating mineral assemblages for the Akdağ volcanics was similar to that of the second stage fractionation model of the Güzüngülü volcanics.

Similar mass balance calculations for the SHO–UK samples did not produce reasonable results ($\Sigma r^2 > 25$), which may indicate that the geochemical trends illustrated in Fig. 8 do not result solely from fractional crystallization processes. This hypothesis can be tested by examining the V/Nd versus Nb systematics of the magmatic rocks (Fig. 11a) because they depend on: (1) the degree of partial melting of the mantle source, and (2) the degree of fractional crystallization (FC), but are relatively independent of: (1) subduction-related source enrichment and (2) source mineralogy (e.g., melts produced by partial melting of garnet-free or garnet-bearing mantle sources). FC of a cpx-dominated assemblage would be resulted in

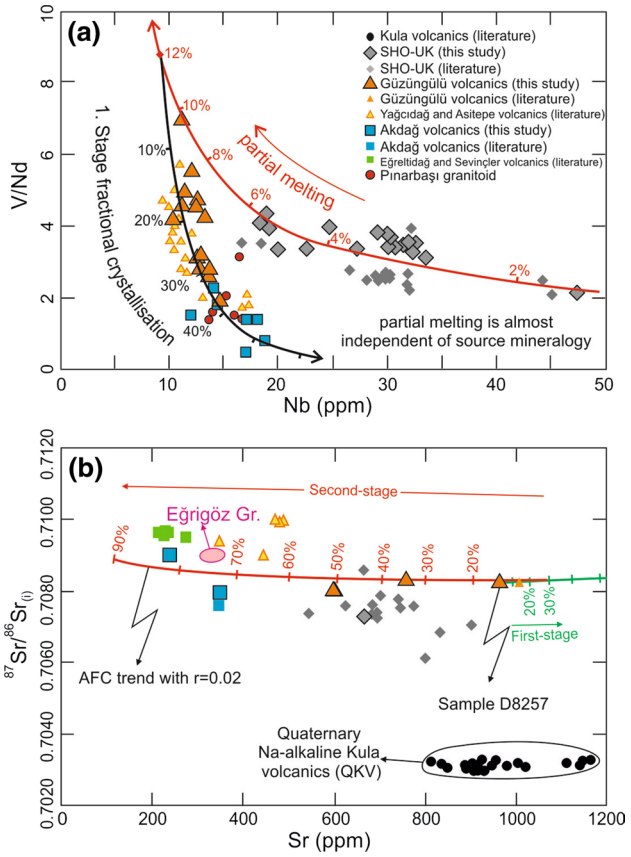

Fig. 11 **a** V/Nd versus Nb, and **b** $^{87}Sr/^{86}Sr_{(i)}$ versus Sr systematics for the magmatic rocks. Clinopyroxene (cpx)-dominated fractional crystallization (FC) model for the HKCA, using the sample D8257, is shown in **a**. Non-modal fractional melting of a metasomatic mantle source with phlogopite harzburgitic mineralogy is also shown in **b**. AFC model on **c** uses cpx-dominated (first stage) and feldspar-dominated (second stage) fractionating mineral assemblages. Geochemical models are produced by using PETROMODELER software (Ersoy 2013)

a sharp decrease in V/Nd ratio with a slight increase in Nb. The best fit to the HKCA data is obtained using an FC trend for an assemblage of olivine (0.1 %) + clinopyroxene (48.1 %) + plagioclase (24.8 %) + amphibole (23.0 %) + magnetite (4.0 %), obtained by using PETROMODELER software (Ersoy 2013). The more acidic samples, together with the Akdağ volcanics, show a trend toward higher Nb concentrations, which can be created by plagioclase- and amphibole-dominated fractionation. The SHO–UK rocks define a distinct, flatter trend that is best modeled by variable melting of a mantle source with far more limited FC. Overall, the relationships in Fig. 11a indicate that the geochemical trends of the HKCA are largely controlled by FC (with or without crustal contamination) processes, while those of the SHO–UK groups are dominated by variable degrees of partial melting (and/or source enrichment) processes.

Crustal contamination

The basement rock units of the volcanic rocks in this study contain some ophiolitic mélange units of the İzmir-Ankara zone, but are dominated by the metamorphic rocks (felsic gneisses and schists) of the MCC that is composed of mid-crustal units exhumed synchronously with the magmatic activity in the region (e.g., Işık et al. 2004). Sr and Nd isotopic ratios obtained from the MCC vary from 0.71655 to 0.86800 and 0.51218 to 0.51283, respectively (Satır and Friedrichsen 1986; Ersoy et al. 2012a; Çoban et al. 2012), which are clearly distinct from the magmatic rocks in the region. Hence, even low-degree contamination of the parental magmas by rocks of the MCC would yield magmas with very high $^{87}Sr/^{86}Sr$ ratios. In contrast, when the Sr isotope data are plotted against the SiO_2 and MgO differentiation indices (Fig. 10c, d), it shows that there is no a significant difference between the $^{87}Sr/^{86}Sr_{(i)}$ of the most primitive and the most evolved samples of any of the rock groups. The Lower Miocene Eğrigöz granitoid and the late Lower–Middle Miocene Asitepe and Yağcıdağ volcanics (located to the south of the region) are, however, characterized by slightly higher $^{87}Sr/^{86}Sr_{(i)}$ ratios (~0.710) than those of the HKCA group (~0.708).

These relationships suggest that crustal contamination played a limited role the in genesis of the rocks. In order to test this hypothesis, AFC processes were modeled on an $^{87}Sr/^{86}Sr$ ratio versus Sr (ppm) diagram (Fig. 11b). In these models of the HKCA group, the average Sr isotopic ratio ($^{87}Sr/^{86}Sr = 0.745725$ and Sr = 150 ppm) of the MCC metamorphic rocks (corrected to 17 Ma) was used as the contaminant composition. Following on from the two-stage fractionation history in the genesis of the HKCA (as described above), a two-step AFC model was constructed. In the first stage, sample D8257 was used as the starting magma composition, together with the first-stage cpx-dominated FC assemblage. This model predicts an initial slight increase in Sr contents. At the start of the second stage, the composition is assumed to reflect 30 % crystallization after the first stage. During the second stage, FC is feldspar-dominated, resulting in a rapid decrease in Sr contents. The near-lateral Sr isotopic variation between the HKCA samples thus constrains *r* (the ratio of assimilated material to crystallized material) to be ~0.02.

The samples of SHO–UK show a negative relationship between $^{87}Sr/^{86}Sr_{(i)}$ and Sr contents (Fig. 11b), which could be taken to indicate that crustal contamination played some role in their genesis. There is, however, no correlation between the $^{87}Sr/^{86}Sr_{(i)}$ of these rocks and their MgO and SiO_2 contents (Fig. 10c, d). Hence, the variable $^{87}Sr/^{86}Sr_{(i)}$ ratios of the SHO–UK rocks are most likely related to their source characteristics, such as source heterogeneity. This interpretation is also supported by irregular relationships

between the differentiation index (SiO_2 or MgO) and the Zr, Ba and Rb concentrations of the mafic lavas (Fig. 8), reflecting some heterogeneity in their source region.

Implications for source characteristics

A common mantle source for HKCA and SHO–UK?

The Neogene to Quaternary volcanic rocks in western Anatolia can be grouped as: (1) HKCA basalt to rhyolites, (2) SHO–UK rocks including lamproites and (3) Na-alkaline OIB-like basaltic rocks (Kula volcanics) (Güleç 1991; Aldanmaz et al. 2000; Yılmaz et al. 2001; Alıcı et al. 2002; Innocenti et al. 2005; Dilek and Altunkaynak 2009; Ersoy et al. 2010a; Karaoğlu et al. 2010). Each group defines a distinct trend on a TAS classification plot (Fig. 6a), indicating that they were derived from distinct sources and/or petrogenetic processes.

The main difficulty in determining the genesis of these distinct magma series, especially groups (1) and (2), is the absence of truly primitive rock samples (with high MgO and Mg#, Ni and Cr contents), particularly for the HKCA rocks. However, basalt samples of the Güzüngülü volcanics with medium-K, calc-alkaline affinity may represent the most primitive samples of the Early–Middle Miocene calc-alkaline volcanism in the region (Fig. 6a, b), although they have high LOI values (up to 6 wt%). Detailed studies on SHO–UK lavas and lamproites in the region, which have high MgO and K_2O contents, show that these rocks were derived from anomalously enriched lithospheric mantle domains (Innocenti et al. 2005; Ersoy et al. 2010b, 2012b; Çoban et al. 2012; Prelević et al. 2012). The Na-alkaline basaltic rocks (group 3) also contain high-MgO rocks, allowing their source to be identified within the asthenospheric mantle (Alıcı et al. 2002). The source characteristics of the HKCA rocks (andesite to rhyolites) have, however, remained controversial, and petrogenetic models for these rocks have been limited (e.g., Yılmaz et al. 2001; Ersoy et al. 2012a). The description of primitive high-MgO basaltic rocks within the Güzüngülü volcanics in this study therefore provides crucial information for determining the origin of the HKCA rocks. Although the most primitive samples of the HKCA (e.g., D8257) have high LOI values (~6 wt%), these rocks still have the potential to reflect the nature of the primitive magma composition (at least, in respect of immobile element contents). Thus, it is important to note these most primitive examples of the HKCA rocks differ from the SHO–UK rocks in both their petrographic and geochemical aspects.

A hybrid origin for the andesitic rocks of the HKCA rocks, via mixing of melts from basaltic (amphibolitic) lower crust and the lithospheric mantle, can be excluded on the basis of the presence of the basaltic rocks of the

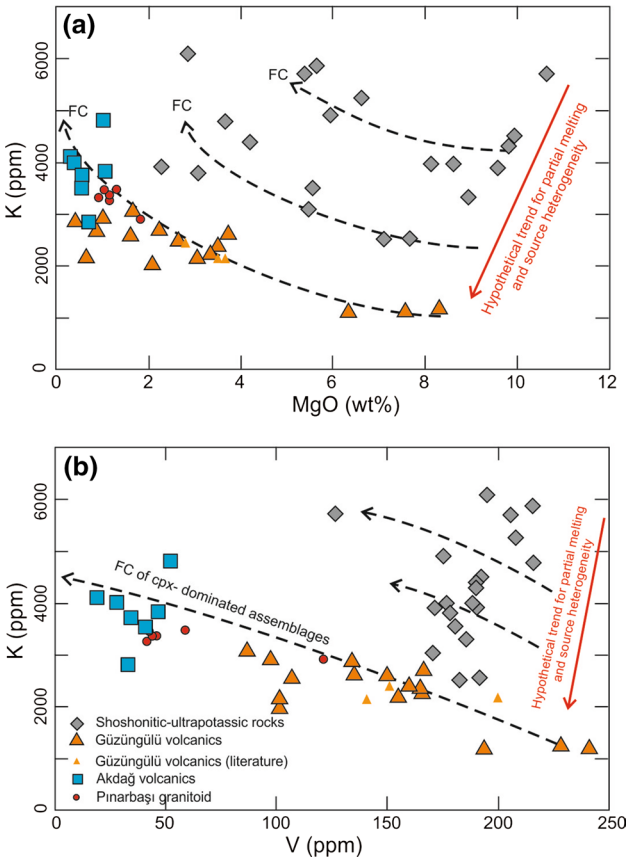

Fig. 12 **a** K (ppm) versus MgO (wt%) and **b** K (ppm) versus V (ppm) plots for magmatic rocks in the region. Also shown are hypothetical trends for partial melting and fractional crystallization

Güzüngülü volcanics in the region, because these rocks have (1) higher MgO (5.9–7.8 wt%) and lower SiO_2 (46.5–48.7 wt%) than melts that produced by experimental melting of amphibolitic sources (MgO = 1.3–2.5 wt% and SiO_2 = 61.7–66.3 wt%; Sen and Dunn 1994) and (2) similar trace element patterns, and Sr–Nd isotopic ratios to those of the lithospheric mantle-derived SHO–UK rocks (Fig. 10). Furthermore, the incompatible–compatible element variations (such as V vs SiO_2) (Fig. 8) show co-linear trends for both groups. This, together with the V/Nb systematics of the two groups (Fig. 11a), suggests that the SHO–UK rocks are the products of low-degree partial melting, while the most primitive HKCA rocks represent the melts from higher-degree partial melting. Based on these observations, we suggest that both groups were derived from a common metasomatized mantle source. This hypothesis is supported by plots of K versus MgO and K versus V (Fig. 12a, b). In this instance, the variation in K contents is interpreted to reflect: (a) different degrees of partial melting of the lithospheric mantle and (b) heterogeneity in that source (with some K enrichment during late stage FC), because K is incompatible in the

mantle mineral assemblages and it is sensitive to variable degrees of subduction-related mantle metasomatism. MgO and V variations, however, largely reflect the degree of olivine and pyroxene FC following extraction of melts from the lithospheric mantle. Thus, the data trends suggest that the SHO–UK series are the products of low-degree partial melting of the mantle source, while the primitive members of the HKCA series represent higher-degree partial melting products of the same mantle (Fig. 12a, b).

Source enrichment processes and mantle composition

Tb/Yb versus La/Yb ratios of the SHO–UK and basaltic to andesitic rocks of the HKCA are shown in Fig. 13. On this plot, the compositions of primitive mantle (PM; Palme and O'Neill 2004), depleted MORB (DMM), depleted DMM (D-DMM) and enriched DMM (E-DMM) (Workman and Hart 2005) are also shown to define enrichment and depletion within the mantle (i.e., mantle array). Partial melting trends for spinel (sp)- and garnet (gt)-facies non-modal batch melting of a DMM source are shown to illustrate the effects of the depth of melting. The most primitive SHO–UK and HKCA samples show a co-linear trend that again suggests that these rocks were derived from a common mantle source by variable degrees of melting. The correlation between the Tb/Yb and the La/Yb ratios of the volcanic rocks suggests they were either formed by partial melting of a garnet-facies (deep) mantle source, or they were derived from mantle that had been metasomatized during the subduction process by material released from a garnet-bearing source (e.g., Avanzinelli et al. 2008). The absence, however, of a positive correlation between Tb/Yb (as a proxy for garnet in the mantle source and in the source from which the fluxing material derived) and Th/Nb (as a proxy for the degree of subduction-related enrichment) suggests that the mantle source region included garnet (inset in Fig. 13). The intersection of the SHO–UK and HKCA data with the mantle array shown in Fig. 13 suggests that the magmas were derived from an anomalously enriched mantle. Indeed, geochemical features such as LILE enrichment over HFSE (relative depletion in Nb and Ta) and high radiogenic Sr contents within the most mafic members of the SHO–UK series have previously been taken to indicate that their sources include the effects of subduction-related enrichment processes (Güleç 1991; Floyd et al. 1998; Aldanmaz et al. 2000; Yılmaz et al. 2001; Innocenti et al. 2005; Ersoy et al. 2010b; Çoban et al. 2012; Prelević et al. 2012).

In general, ultrapotassic rocks along the Alpine-Himalayan system are characterized by the high whole-rock MgO (and other compatible elements) and K_2O (and other incompatible elements) contents, and the presence of xenocrystic olivines with high Fo contents and high

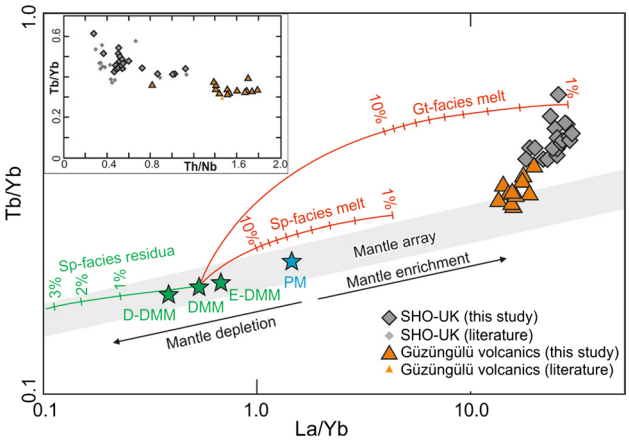

Fig. 13 Tb/Yb versus La/Yb plot for magmatic rocks in the region. Also shown in **a** are primitive mantle (PM; Palme and O'Neill 2004), depleted MORB (DMM), depleted DMM (D-DMM) and enriched DMM (E-DMM) (Workman and Hart 2005). Mineral modal abundances (melt modes in *parentheses*) for spinel (sp)- and garnet (gt)-facies non-modal batch melting models are: olivine 0.53 (-0.06) + orthopyroxene 0.27 (0.28) + clinopyroxene 0.17 (0.67) + spinel 0.03 (0.11) (Kinzler 1997) and olivine 0.60 (0.03) + orthopyroxene 0.20 (−0.16) + clinopyroxene 0.10 (0.88) + garnet 0.10 (0.09) (Walter 1998). The *inset diagram* shows the variations of Tb/Yb with Th/Nb ratio of the rocks. Geochemical models are produced by using PETROMODELER software (Ersoy 2013)

Cr# spinel inclusions, that suggest they were derived from melting of highly depleted harzburgitic mantle domains which were anomalously enriched by subduction-related processes (e.g., Prelević et al. 2010). Semiz (2010) and Prelević et al. (2010) also reported mantle xenocrystic olivines in the Ilıcaksu lamproite from the SHO–UK rocks in the study area considered here. Recently, Condamine and Médard (2014) have also shown experimentally that ultrapotassic melts can be generated by melting of phlogopite-bearing mantle, and other experimental studies have previously shown that ultrapotassic (lamproitic) magmas can coexist with garnet harzburgite (Sato 1997).

These mantle enrichment events have been ascribed to subduction of oceanic slices and sediments (Peccerillo and Martinotti 2006; Gao et al. 2007; Prelević et al. 2012, 2013; Tommasini et al. 2011), and/or subduction of continental crustal slices during imbrication of crustal blocks during continent–continent collision (Çoban et al. 2012; Ersoy et al. 2012b; Ersoy and Palmer 2013). The latter hypothesis is supported by the observation (Ersoy et al. 2012b) that the mantle source composition of the Miocene SHO–UK volcanic rocks is comparable to crustally contaminated mantle peridotites from the Ulten Zone Alpine peridotites (Marocchi et al. 2007; Rampone and Morten 2001; Scambelluri et al. 2006; Tumiati et al. 2007). In addition, recent boron isotope studies of the MCC also support the hypothesis

that imbrication and partial subduction of tectonic slices of continental crust, represented by metamorphic rocks of the MCC, resulted in mobilization of fluid mobile elements that may have led to metasomatism of western Anatolian mantle domains (Floyd et al. 1998; Yücel-Öztürk et al. 2015).

Partial melting and magma generation

When the observations above are coupled with our findings, it appears that the SHO–UK rocks were derived from low-degree partial melting of an anomalously enriched mantle with phlogopite-garnet harzburgite mineralogy with geochemical characteristics similar to those of the continentally metasomatized Ulten Zone Peridotites (UZP) and that the HKCA were derived from higher-degree partial melting of the same source. Hence, the UZP is viable as a starting mantle composition for melting models.

The effects of both partial melting and fractional crystallization processes can be simulated using an incompatible element (such as Nb) and a compatible element (for cpx-dominated fractionation, such as V). Cpx-dominated FC results in a sharp decrease in V/Nd ratio over a limited Nb range (as defined by the HKCA data), while partial melting results in a shallower negative correlation between V/Nd and Nb (as defined by the SHO–UK data) (Fig. 11a). Thus, the geochemical variations of the SHO–UK rocks can be reproduced by low-degree partial melting of the mantle source with UZP average composition and phlogopite-garnet harzburgite mineralogy. Note that these ratios are almost independent of the degree of source enrichment and source mineralogy because these elements are relatively fluid-immobile.

During cpx-dominated FC, the Sr/V ratio increases sharply with a slight decrease in Nb, while fractionation of a feldspar-dominated assemblage decreases the Sr/V ratio with very little impact on Nb (Fig. 14a). Thus, the genesis of HKCA rocks appears to be most compatible with ~10–20 % partial melting of a UZP-like mantle source followed by a two-stage FC process. In contrast, the SHO–UK rocks appear to have formed by only ~3–5 % partial melting of the same UZP-like source and much lower degrees of subsequent FC.

It is important to recognize, however, that while these models clearly support the hypothesis that SHO–UK series were derived from substantially lower degrees of mantle partial melting than the HKCA rocks, the absolute magnitudes of partial melting depend strongly on the precise composition of the mantle source. For example, a model of the Tb/Yb versus Ce/Yb ratios of the magmatic rocks (Fig. 14b) does not produce a melting trend that passes through the data. This is likely because the Ce/Yb ratio is strongly controlled by the degree of enrichment of the mantle source. If, however, the mantle source beneath western Anatolia was more enriched in Ce than the UZP rocks, a parallel partial melting model curve could be produced that would pass through the data and would still support the hypothesis that the SHO–UK rocks are low-degree melting products than the HKCA. The melting models do, however, indicate that the mantle source contains ~3 % garnet, because higher garnet amounts in the source would resulted in a much steeper rise in Tb/Yb ratios than the trend shown by the volcanics, and vice versa.

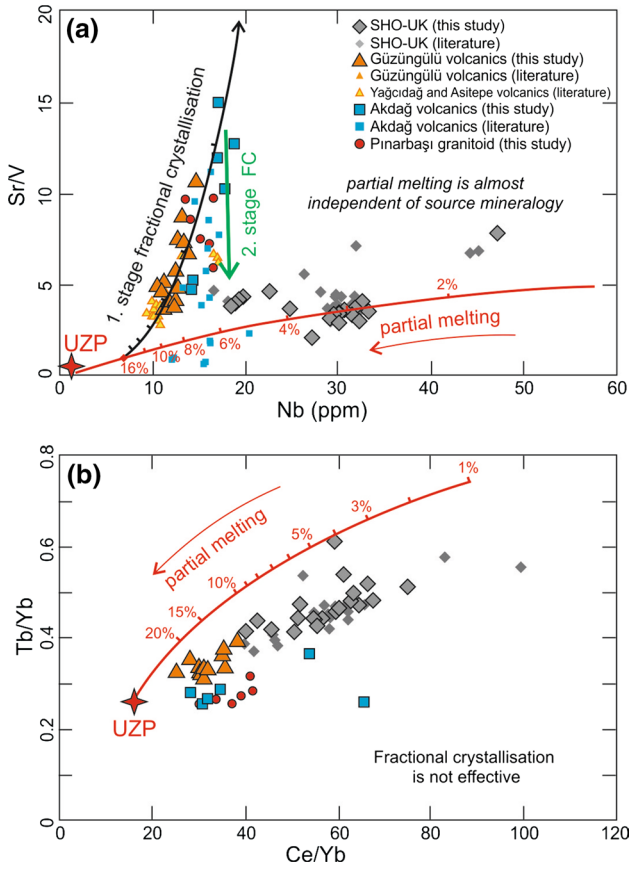

Fig. 14 **a** Sr/V versus Nb (ppm) and **b** Tb/Yb versus Ce/Yb plots for the magmatic rocks in the region. Non-modal batch melting models use the average composition of the Ulten Zone Peridotites (UZP; Marocchi et al. 2007; Rampone and Morten 2001; Scambelluri et al. 2006; Tumiati et al. 2007) with phlogopite harzburgite mineralogy as starting material. Mineral modal abundances (melt modes in *parentheses*) for phlogopite harzburgite is olivine 0.69 (0.15) + orthopyroxene 0.10 (0.17) + clinopyroxene 0.03 (0.27) + garnet 0.03 (0.05) + phlogopite 0.14 (0.35) + spinel 0.01 (0.01) (from Williams et al. 2004). Fractional crystallization models with clinopyroxene-dominated assemblage (olivine 0.1 % + clinopyroxene 48.1 % + plagioclase 24.8 % + amphibole 23 % + magnetite 4 %) are shown in **a**, by using 12, 12 and 16 % partial melt compositions, respectively. The effects of second-stage feldspar-dominated fractionation are also shown in **a**, as this assemblage affects the Sr/V ratio of the melt. Geochemical models are produced by using PETROMODELER software (Ersoy 2013)

Time-dependent chemical variation

The well-studied potassic to ultrapotassic magmatic rocks in Italy show a general shift from ultrapotassic to shoshonitic and then calc-alkaline compositions (Conticelli et al. 2011, 2013 and references therein). This case is mostly interpreted to be resulted from melting of metasomatic veins and then the surrounding peridotites, to produce ultrapotassic and calc-alkaline, respectively (e.g., Foley 1992). Taking into account the age data for the western Anatolian Miocene magmatism, it is apparent that the geochemical features of the magmatic products changed with time as well. However, in the case of western Anatolia, the former (Lower Miocene) magmatic rocks are dominantly HKCA (HKCA) in character, while those of the following (Middle Miocene) magmatism show both ultrapotassic (and shoshonitic; SHO–UK) and HKCA affinities, that is an opposite with the Italian magmatism.

This circumstance may be related with the local geological evolution of the western Anatolia, where the Miocene magmatism was closely associated with the extensional tectonics. Late Oligocene–Early Miocene times in the region marks the changing from compressional to extensional tectonics, along which the over-thickened orogenic crust begun to rapidly thinning with exhumation of the metamorphic rocks MCC (Işık et al. 2004; Ersoy et al. 2008; 2010b; 2012b; Karaoğlu et al. 2010). Rapid exhumation of the MCC was accompanied by wide-spread HKCA dacitic to rhyolitic magmatism at 21–18 Ma (such as Akdağ volcanics in this study and granitic plutons). This might led to high-degrees of partial melting and to extensive fractional crystallization of the produced magmas in a relatively thick crust. During the 16–14 Ma, HKCA volcanics changed from dacitic to rhyolitic into the more intermediate compositions such as andesite and basalts; and the high-MgO SHO–UK magmas begun to rise to surface, compatible with the crustal thinning with time. In this model, the HKCA volcanic rocks, forming the larger volcanic edifices in the region, may be considered as the high-degree melting products of heterogeneously metasomatized common mantle source. The ultrapotassic volcanic units, with smaller outcrops, on the other hand, may represent the low-degree melt pockets, produced in the course of extension-driven magmatic activity. Therefore, this model is compatible with the relative amounts of large-volume calc-alkaline magmatic rocks and the small-volume ultrapotassic rocks.

Conclusions

The magmatic rocks exposed around the Simav graben include an association of (1) Lower–Middle Miocene HKCA basalt to rhyolite and (2) Middle Miocene high-MgO shoshonitic–ultrapotassic (SHO–UK) series. All the HKCA samples, together those from the surrounding area, share similar geochemical characteristics with enrichments of LILE and LREE over HFSE and high Sr isotopic ratios (0.708–0.710). The samples of the SHO–UK group with high incompatible trace element contents share common geochemical features with the orogenic ultrapotassic (or lamproitic) rocks emplaced along the Alpine-Himalayan belt.

Geochemical models using trace element abundances and ratios with Sr–Nd isotopic compositions indicate that the SHO–UK and HKCA groups were derived from a common mantle source which had been metasomatized and enriched by continental materials during partial subduction of the metamorphic slices of the MCC during continent–continent collision, preceding the extensional tectonics. The geochemical features of the most primitive basaltic rocks of the HKCA group in the region (described here for the first time) suggest they were derived by higher degrees of melting of the orogenic mantle source than the SHO–UK series and that these melts then underwent two-stage fractional crystallization (cpx-dominated at first, followed by feldspar-dominated) to form the basalt to rhyolite series. Wide-spread occurrence of these earlier magmatic rocks is related to the high-degree melting of the mantle domains beneath the rapidly extended and thinned of previously over-thickened orogenic crust. The HKCA magmatism was then accompanied by the small-volume production of the SHO–UK rocks, representing low-degree partial melts from similar mantle source. The ongoing crustal thinning led to rise of these relatively undifferentiated magmas to the surface.

Acknowledgments This study forms part of a Ph.D. study by the first author and has been encouraged by a research project supported by Pamukkale University (Project No. 2008MHF003). We would like to thank Paul Schroeder who facilitated the visit of the first author to the University of Georgia, Athens, USA, and Chris Fleisher for his assistance in performing the microprobe analyses. Tyrone Rooney is thanked for his contribution to an earlier version of the manuscript. Michael F. Roden is acknowledged for his English editing and critical comments that contributed to the improvement of this paper.

References

Akal C (2008) K-richterite–olivine–phlogopite–diopside–sanidine lamproites from the Afyon volcanic province, Turkey. Geol Mag 145:570–585

Aldanmaz E, Pearce JA, Thirlwall MF, Mitchell JG (2000) Petrogenetic evolution of late Cenozoic, post-collision volcanism in western Anatolia Turkey. J Volcanol Geotherm Res 102:67–95

Alıcı P, Temel A, Gourgaud A (2002) Pb–Nd–Sr isotope and trace element geochemistry of Quaternary extension-related alkaline volcanism: a case study of Kula region (western Anatolia, Turkey). J Volcanol Geotherm Res 115(3–4):487–510

Altherr R, Meyer HP, Holl A, Volker F, Alibert C, McCulloch MT, Majer V (2004) Geochemical and Sr–Nd–Pb isotopic

characteristics of Late Cenozoic leucite lamproites from the East European Alpine belt (Macedonia and Yugoslavia). Contrib Mineral Petrol 147:58–73

Altunkaynak Ş, Genç ŞC (2008) Petrogenesis and time-progressive evolution of the Cenozoic continental volcanism in the Biga Peninsula, NW Anatolia (Turkey). Lithos 102:316–340

Altunkaynak Ş, Sunal G, Aldanmaz E, Genç CŞ, Dilek Y, Furnes H, Foland KE, Yang J, Yıldız M (2012) Eocene Granitic Magmatism in NW Anatolia (Turkey) revisited: new implications from comparative zircon SHRIMP U-Pb and ^{40}Ar–^{39}Ar geochronology and isotope geochemistry on magma genesis and emplacement. Lithos 155:289–309

Armstrong JT (1988) Quantitative analysis of silicate and oxide materials: comparison of Monte Carlo, ZAF, and phi–rho–z procedures. Microbeam Anal 23:239–246

Avanzinelli R, Elliot T, Tommasini S, Conticelli S (2008) Constraints on the genesis of potassium-rich Italian volcanic rocks from U/Th disequilibrium. J Petrol 49:195–223

Avanzinelli R, Lustrino M, Mattei M, Melluso L, Conticelli S (2009) Potassic and ultrapotassic magmatism in the circum-Tyrrhenian region: significance of carbonated pelitic vs. pelitic sediment recycling at destructive plate margins. Lithos 113:213–227

Bacon CR, Hirschmann MM (1988) Mg/Mn partitioning as a test for equilibrium between coexisting Fe–Ti oxides. Am Mineral 73:57–61

Bailey JC, Jensen ES, Hansen A, Kann ADJ, Kann K (2009) Formation of heterogeneous magmatic series beneath North Santorini, South Aegean island arc. Lithos 110:20–36

Benito R, Lopez-Ruiz J, Cebria JM, Mertogen J, Doblas M, Oyarzun R, Demaiffe D (1999) Sr and O isotope constraints on source and crustal contamination in the high-K calc-alkaline and shoshonitic Neogene volcanic rocks of SE Spain. Lithos 46:773–802

Buettner A, Kleinhanns IC, Rufer D, Hunziker JC, Villa IM (2005) Magma generation at the easternmost section of the Hellenic arc: Hf, Nd, Pb and Sr isotope geochemistry of Nisyros and Yali volcanoes (Greece). Lithos 83:29–46

Chakrabarti R, Basu AR, Ghatak A (2012) Chemical geodynamics of Western Anatolia. Int Geol Rev 54:227–248

Çiftçi NB, Bozkurt E (2009) Facies and evolution of the Miocene–recent sedimentary fill of the Gediz Graben, SW Turkey. Sediment Geol 216:49–79

Çoban H, Flower MFJ (2006) Mineral phase compositions in silica-undersaturated 'leucite' lamproites from the Bucak area, Isparta, SW Turkey. Lithos 89:275–299

Çoban H, Karacık Z, Ece ÖI (2012) Source contamination and tectonomagmatic signals of overlapping Early to Middle Miocene orogenic magmas associated with shallow continental subduction and asthenospheric mantle flows in Western Anatolia: a record from Simav (Kütahya) region. Lithos 140–141:119–141

Condamine P, Médard E (2014) Experimental melting of phlogopite-bearing mantle at 1.0 GPa: implications for potassic magmatism. Earth Planet Sci Lett 397:80–92

Conticelli S, Guarnieri L, Farinelli A, Mattei M, Avanzinelli R, Bianchini G, Boari E, Tommasini S, Tiepolo M, Prelević D, Venturelli G (2009) Trace elements and Sr–Nd–Pb isotopes of K-rich, shoshonitic, and calc-alkaline magmatism of the Western Mediterranean Region: genesis of ultrapotassic to calc-alkaline magmatic associations in a post-collisional geodynamic setting. Lithos 107:68–92

Conticelli S, Avanzinelli R, Marchionni S, Tommasini S, Melluso L (2011) Sr–Nd–Pb isotopes from the Radicofani Volcano, Central Italy: constraints on heterogeneities in a veined mantle responsible for the shift from ultrapotassic shoshonite to basaltic andesite magmas in a post-collisional setting. Mineral Petrol 103(1–4):123–148

Conticelli S, Avanzinelli R, Poli G, Braschi E, Giordano G (2013) Shift from lamproite-like leucititic rocks: Sr–Nd–Pb isotope data from the Monte Cimino volcanic complex vs. the Vico stratovolcano, Central Italy. Chem Geol 353:246–266

Deer WA, Howie RA, Zussman J (1966) An introduction to the rock forming minerals. Longman, London

Dilek Y, Altunkaynak Ş (2009) Geochemical and temporal evolution of Cenozoic magmatism in western Turkey: mantle response to collision, slab breakoff, and lithospheric tearing in an orogenic belt. Geol Soc London Spec Publ 311:213–233

Duggen S, Hoernle K, Bogaard PVD, Garbe-Schönberg D (2005) Post-collisional transition from subduction to intraplate-type magmatism in the westernmost Mediterranean: evidence for continental-edge delamination of subcontinental lithosphere. J Petrol 46:1155–1201

Ercan T, Satır M, Sevin D, Türkecan A (1996) Batı Anadolu'daki Tersiyer ve Kuvaterner yaşlı volkanik kayaçlarda yeni yapılan radyometrik yaş ölçümlerinin yorumu. MTA Dergisi 119:103–112

Ersoy EY (2013) PETROMODELER (Petrological Modeler): a Microsoft® Excel© spreadsheet program for modeling melting, mixing, crystallisation and assimilation processes in magmatic systems. Turk J Earth Sci 22:115–125

Ersoy EY, Helvacı C (2007) Stratigraphy and geochemical features of the Early Miocene bimodal (ultrapotassic and calc-alkaline) volcanic activity within the NE-trending Selendi Basin, Western Anatolia, Turkey. Turk J Earth Sci 16:117–139

Ersoy EY, Palmer MR (2013) Eocene-Quaternary magmatic activity in the Aegean: implications for mantle metasomatism and magma genesis in an evolving orogeny. Lithos 180–181:5–24

Ersoy EY, Helvacı C, Sözbilir H, Erkül F, Bozkurt E (2008) A geochemical approach to Neogene–Quaternary volcanic activity of western Anatolia: an example of episodic bimodal volcanism within the Selendi Basin, Turkey. Chem Geol 255:265–282

Ersoy EY, Helvacı C, Sözbilir H (2010a) Tectono-stratigraphic evolution of the NE–SW-trending superimposed Selendi basin: implications for late Cenozoic crustal extension in Western Anatolia, Turkey. Tectonophysics 488:210–232

Ersoy EY, Helvacı C, Palmer MR (2010b) Mantle source characteristics and melting models for the early-middle Miocene mafic volcanism in Western Anatolia: implications for enrichment processes of mantle lithosphere and origin of K-rich volcanism in post collisional settings. J Volcanol Geotherm Res 198:112–128

Ersoy EY, Helvacı C, Palmer MR (2011) Stratigraphic, structural and geochemical features of the NE–SW-trending Neogene volcano-sedimentary basins in western Anatolia: implications for associations of supradetachment and transtensional strike–slip basin formation in extensional tectonic setting. J Asian Earth Sci 41:159–183

Ersoy EY, Helvacı C, Palmer MR (2012a) Petrogenesis of the Neogene volcanic units in the NE–SW-trending basins in western Anatolia, Turkey. Contrib Mineral Petrol 163:379–401

Ersoy EY, Helvacı C, Uysal İ, Karaoğlu Ö, Palmer MR, Dindi F (2012b) Petrogenesis of the Miocene volcanism along the İzmir–Balıkesir Transfer Zone in western Anatolia, Turkey: implications for origin and evolution of potassic volcanism in post-collisional areas. J Volcanol Geotherm Res 241–242:21–38

Floyd PA, Helvacı C, Mittwede SK (1998) Geochemical discrimination of volcanic rocks associated with borate deposits: an exploration tool? J Geochem Explor 60:185–220

Foley SF (1992) Petrological characterization of the source components of potassic magmas: geochemical and experimental constraints. Lithos 28:187–204

Foley SF, Venturelli G, Green DH, Toscani L (1987) The ultrapotassic rocks: characteristics, classification, and constraints for petrogenetic models. Earth Sci Rev 24:81–134

Francalanci L, Innocenti F, Manetti P, Savaşçin MY (2000) Neogene alkaline volcanism of the Afyon-Isparta area, Turkey: petrogenesis and geodynamic implications. Mineral Petrol 70:285–312

Fuhrman ML, Lindsley DH (1988) Ternary-feldspar modeling and thermometry. Am Mineral 73:201–215

Fytikas M, Innocenti F, Manetti P, Mazzuoli R, Peccerillo A, Villari L (1984) Tertiary to Quaternary evolution of volcanism in the Aegean region. Geol Soc Lond Spec Publ 17:687–699

Gao Y, Hou Z, Kamber BS, Wei R, Meng X, Zhao R (2007) Lamproitic rocks from a continental collision zone: evidence for recycling of subducted Tethyan Oceanic sediments in the mantle beneath southern Tibet. J Petrol 48:729–752

Güleç N (1991) Crust-mantle interaction in western Turkey: implications from Sr and Nd isotope geochemistry of Tertiary and Quaternary volcanics. Geol Mag 128:417–435

Gülmez F, Genç ŞC, Keskin M, Tüysüz O (2012) A post-collision slab-breakoff model for the origin of the Middle Eocene magmatic rocks of the Armutlu–Almacık belt, NW Turkey and its regional implications. Geol Soc London Spec Publ 372:107–139

Guo Z, Liu J, Hertogen J, Pasteels P, Boven A, Punzalan L, He H, Luo X, Zhang W (2005) Potassic magmatism in Western Sichuan and Yunnan Provinces, SE Tibet, China: petrological and geochemical constraints on petrogenesis. J Petrol 46:33–78

Helvacı C, Alonso RN (2000) Borate deposits of Turkey and Argentina; a summary and geological comparison. Turk J Earth Sci 24:1–27

Helvacı C, Ersoy EY, Sözbilir H, Erkül F, Sümer Ö, Uzel B (2009) Geochemistry and $^{40}Ar/^{39}Ar$ geochronology of Miocene volcanic rocks from the Karaburun Peninsula: implications for amphibole-bearing lithospheric mantle source, Western Anatolia. J Volcanol Geotherm Res 185:181–202

Innocenti F, Agostini S, Di Vincenzo G, Doglioni C, Manetti P, Savaşçın MY, Tonarini S (2005) Neogene and Quaternary volcanism in Western Anatolia: magma sources and geodynamic evolution. Mar Geol 221:97–421

Işık V, Seyitoğlu G, Çemen İ (2003) Ductile–brittle transition along the Alaşehir detachment fault and its structural relationship with the Simav detachment fault, Menderes Massif, Western Turkey. Tectonophysics 374:1–18

Işık V, Tekeli O, Seyitoğlu G (2004) The $^{40}Ar/^{39}Ar$ age of extensional ductile deformation and granitoid intrusions in the northern Menderes core complex: implications for the initiation of extensional tectonics in western Turkey. J Asian Earth Sci 23:555–566

Karacık Z, Yılmaz Y, Pearce JA (2007) The Dikili–Çandarlı volcanics, western Turkey: magmatic interactions as recorded by petrographic and geochemical features. Turk J Earth Sci 16:493–522

Karaoğlu Ö, Helvacı C, Ersoy EY (2010) Petrogenesis and $^{40}Ar/^{39}Ar$ geochronology of the volcanic rocks of the Uşak-Güre basin, western Turkey. Lithos 119:193–210

Kinzler RJ (1997) Melting of mantle peridotite at pressures approaching the spinel to garnet transition: application to mid-ocean ridge basalt petrogenesis. J Geophys Res 102:853–874

Kürkçüoğlu B, Furman T, Hanan B (2008) Geochemistry of postcollisional mafic lavas from the North Anatolian Fault zone, Northwestern Turkey. Lithos 101:416–434

Leake BE, Woolley AR, Arps CES, Birch WD, Gilbert MC (1997) Nomenclature of amphiboles: report of the subcommittee on amphiboles of the International Mineralogical Association, commission on new minerals and mineral names. Am Mineral 82:1019–1037

LeMaitre RW (2002) Igneous rocks: a classification and glossary of terms: recommendations of the International Union of Geological Sciences. Subcommission on the systematics of igneous rocks. Cambridge Univ Press, Cambridge

Lustrino M, Wilson M (2007) The circum-Mediterranean anorogenic Cenozoic igneous province. Earth Sci Rev 81:1–65

Lustrino M, Duggen S, Rosenberg CL (2011) The Central-Western Mediterranean: anomalous igneous activity in an anomalous collisional tectonic setting. Earth Sci Rev 104:1–40

Maniar PD, Piccoli PM (1989) Tectonic discrimination of granitoids. Geol Soc Am Bull 101:635–643

Marocchi M, Hermann J, Morten L (2007) Evidence for multi-stage metasomatism of chlorite–amphibole peridotites (Ulten Zone, Italy): constraints from trace element compositions of hydrous phases. Lithos 99:85–104

Morimoto N (1988) Nomenclature of pyroxenes. Bull Mineral 111:535–550

Nimis P (1995) A clinopyroxene geobarometer for basaltic systems based on crystal structure modeling. Contrib Mineral Petrol 121:115–125

Ozpinar Y, Semiz B, Schroeder PA (2013) Zeolites in mafic pyroclastic rocks from the Sandikli-Afyonkarahisar region, Turkey. Clays Clay Miner 61–3:177–192

Palme H, O'Neill HSC (2004) Cosmochemical estimates of mantle composition. In: Holland HD, Turekian KK (eds) Treatise on geochemistry, vol 2. Elsevier, Amsterdam, pp 1–38

Peccerillo A, Martinotti G (2006) The Western Mediterranean lamproitic magmatism: origin and geodynamic significance. Terra Nova 18:109–117

Pe-Piper G, Piper DJW (1989) Spatial and temporal variations in late Cenozoic back-arc volcanic rocks, Aegean Sea region. Tectonophysics 196:113–134

Petrelli M, Poli G, Perugini D, Peccerillo A (2005) Petrograph: new software to visualize, model, and present geochemical data in igneous petrology. Geochem Geophys Geosyst 6:Q07011

Prelević D, Foley SF, Romer RL, Cvetković V, Downes H (2005) Tertiary ultrapotassic volcanism in Serbia: constraints on petrogenesis and mantle source characteristics. J Petrol 46:1443–1487

Prelević D, Foley SF, Romer R, Conticelli S (2008) Mediterranean Tertiary lamproites derived from multiple source components in post collisional geodynamics. Geochim Cosmochim Acta 72:2125–2156

Prelević D, Akal C, Romer RL, Foley F (2010) Lamproites as indicators of accretion and/or shallow subduction in the assembly of south-western Anatolia, Turkey. Terra Nova 22–6:443–452

Prelević D, Akal C, Foley F, Romer RL, Stracke A, van den Bogaard P (2012) Ultrapotassic mafic rocks as geochemical proxies for post-collisional dynamics of orogenic lithospheric mantle: the case of southwestern Anatolia, Turkey. J Petrol 53:1019–1055

Prelević D, Jacob DE, Foley SF (2013) Recycling plus: a new recipe for the formation of Alpine–Himalayan orogenic mantle lithosphere. Earth Planet Sci Lett 362:187–197

Prelević D, Akal C, Romer RL, Mertz-Kraus R, Helvacı C (2015) Magmatic response to slab tearing: constraints from the Afyon Alkaline Volcanic Complex, Western Turkey. J Petrol 56–3:527–562

Purvis M, Robertson A, Pringle M (2005) Ar-40–Ar-39 dating of biotite and sanidine in tuffaceous sediments and related intrusive rocks: implications for the Early Miocene evolution of the Gördes and Selendi basins, W Turkey. Geodin Acta 18:239–253

Putirka K (2008) Thermometers and barometers for volcanic systems. Rev Mineral Geochem 69:61–120

Putirka K, Mikaelian H, Ryerson F, Shaw H (2003) New clinopyroxene liquid thermobarometers for mafic, evolved and volatile-bearing lava compositions, with applications to lavas from Tibet and the Snake River Plain, Idaho. Am. Mineral 88:1542–1554

Rampone E, Morten L (2001) Records of crustal metasomatism in the garnet peridotites of the Ulten zone (Upper Austroalpine, Eastern Alps). J Petrol 42:207–219

Richardson-Bunbury JM (1996) The Kula volcanic field, western Turkey: the development of a Holocene alkali basalt province and the adjacent normal-faulting graben. Geol Mag 133:275–283

Rieder M, Cavazzini G, Yakonov YSD, Frank VA, Gottardi D (1999) Nomenclature of micas. Mineral Mag 63:267–279

Ring U, Collins AS (2005) U–Pb SIMS dating of synkinematic granites: timing of core-complex formation in the northern Anatolide belt of western Turkey. J Geol Soc London 162:289–298

Roden MF, Patiño-Douce AE, Jagoutz E, Laz'ko EE (2006) High pressure petrogenesis of Mg-rich garnet pyroxenites from Mir kimberlite, Russia. Lithos 90:77–91

Romer RL, Forster H-J, Breitkreuz C (2001) Intracontinental extensional magmatism with a subduction fingerprint: the late Carboniferous Halle Volcanic Complex (Germany). Contrib Mineral Petrol 141:201–221

Satır M, Friedrichsen H (1986) The origin and evolution of the Menderes Massif, W-Turkey: a rubidium/strontium and oxygen isotope study. Geol Rund 75:703–714

Sato K (1997) Melting experiments on a synthetic olivine lamproite composition up to 8 GPa: implication to its petrogenesis. J Geophys Res 102:751–764

Scambelluri M, Hermann J, Morten L, Rampone E (2006) Melt- versus fluid-induced metasomatism in spinel to garnet wedge peridotites (Ulten Zone, Eastern Italian Alps): clues from trace element and Li abundances. Contrib Mineral Petrol 151:372–394

Semiz B (2010) Mineral-chemistry of Ilicaksu lamproitic dykes from Gediz region, western Anatolia. Abstr Prog GSA Ann Meet 33:27

Semiz B, Özpınar Y, Helvacı C (2010) Geochemistry of the Pinarbasi granite (Gediz-Kutahya-Western Anatolia). In: Goldschmidt conference in geochimica and cosmochimica acta, 13–18 June, Knoxville, Tennessee, USA, p A933

Semiz B, Çoban H, Roden MF, Özpınar Y, Flower MFJ, McGregor H (2012) Mineral composition in cognate inclusions in Late Miocene–Early Pliocene potassic lamprophyres with affinities to lamproites from the Denizli region, Western Anatolia, Turkey: implications for uppermost mantle processes in a back-arc setting. Lithos 134–135:253–272

Sen C, Dunn T (1994) Dehydration melting of a basaltic composition amphibolite at 1.5 and 2.0 GPa: implications for the origin of adakites. Contrib Mineral Petrol 117:394–409

Şengör AMC, Yılmaz Y (1981) Tethyan evolution of Turkey: a plate tectonic approach. Tectonophysics 75:181–241

Seyitoğlu G, Anderson D, Nowell G, Scott B (1997) The evolution from Miocene potassic to Quaternary sodic magmatism in western Turkey: implications for enrichment processes in the lithospheric mantle. J Volcanol Geotherm Res 76:127–147

Thompson RN, Gibson SA (2000) Transient high temperatures in mantle plume heads inferred from magnesian olivines in Phanerozoic picrites. Nature 407:502–506

Tommasini S, Avanzinelli R, Conticelli S (2011) The Th/La and Sm/La conundrum of the Tethyan realm lamproites. Earth Planet Sci Lett 301:469–478

Tumiati S, Godard G, Martin S, Klötzli U, Monticelli D (2007) Fluid-controlled crustal metasomatism within a high-pressure subducted mélange (Mt. Hochwart, Eastern Italian alps). Lithos 94:148–167

Williams HM, McCammon C, Peslier AH, Halliday AN, Teutsch N, Levasseur S, Burg JP (2004) Iron isotope fractionation and the oxygen fugacity of the mantle. Science 304:1656–1659

Workman RK, Hart SR (2005) Major and trace element composition of the depleted MORB mantle (DMM). Earth Planet Sci Lett 231:53–72

Yanev Y, Boev B, Doglioni C, Innocenti F, Manetti P, Pecskay Z, Tonarini S, D'Orazio M (2008) Late Miocene–Pleistocene potassic volcanism in the Republic of Macedonia. Mineral Petrol 94:45–60

Yılmaz Y, Genç SC, Karacık Z, Altunkaynak Ş (2001) Two contrasting magmatic associations of NW Anatolia and their tectonic significance. J Geodyn 31(3):243–271

Yücel-Öztürk Y, Helvacı C, Palmer MR, Ersoy EY, Freslon N (2015) Origin and significance of tourmalinites and tourmaline-bearing rocks of Menderes Massif, western Anatolia, Turkey. Lithos 218–219:22–36

Zellmer GF, Turner SP, Hawkesworth CJ (2000) Timescales of destructive plate margin magmatism: new insights from Santorini, Aegean Volcanic Arc. Earth Planet Sci Lett 174:265–281